University of Glasgow

UKJ EEL

UK Japan Engineering Education League

5th UK-Japan Engineering Education League Workshop

7th-8th September 2017
James Watt South Building,
University of Glasgow
Glasgow, UK

We would like to thank our Sponsors for the event

University of Glasgow

EPSRC

Engineering and Physical Sciences Research Council

energy technology partnership

1. Foreword

We are gathered in Glasgow for the 5th meeting of the UK Japan Engineering Education League, following a series of "home and away" meetings. The UKJEEL was formed at a meeting at Tokyo Tech in March 2014 with the objective of advancing engineering education and mobility between our two countries. The impetus of its foundation was the 150th anniversary of the arrival of the Choshu Five to the UK: the earliest example of young Japanese students coming to study at UK universities. Subsequently all five played major roles in the creation of a modern Japanese state during the Meiji period.

Glasgow is a particularly significant venue, both for its pivotal place in the history of engineering (the James Watt building in which we meet marks seminal work on energy). Japanese students came to Glasgow University attracted by Lord Kelvin and other famous professors and by the industrial activities of Glasgow, particularly ship building. Many famous ships of the Imperial Japanese Navy were built on the Clyde, promoting a deep respect between our countries. We should not forget the story of the export of Scottish whiskey to Japan which has been a long standing bond between us.

We are meeting in the spirit of mutual understanding and cooperation which we hope will serve to generate lifelong friendships and professional contacts, between both individuals and institutions, and between students and faculty members.

Enjoy our time together!

Professor Roderick A Smith, FREng, ScD

Formerly Chief Scientific Advisor Department for Transport

Past President Institution of Mechanical Engineers

Chair Future Rail Research Centre Imperial College London, SW7 2BX

Contents

2. List of Abstracts

List of Abstracts

2. Programme

September 6 Wednesday

Arrive in Glasgow

September 7 Thursday

9:00-9:40	Registration and Coffee, James Watt South (JWS), Room 526 Foyer Posters to go on poster boards set up in Room 526, available from 9:00
9:40-9:55	Welcome and Introduction to Glasgow by Professor Jane Duckett, International Dean for East Asia, University of Glasgow, Rm 375
10:00-10:30	Group photograph, *venue weather dependent*
10:30-10:40	Opening Session by Professor David Cumming, Head of School of Engineering, University of Glasgow, Rm 375
10:40-10:55	Welcome to UKJEEL by Professor Roderick Smith, Imperial College London, Rm 375
11:00-12:00	Oral Short 2-3 min student presentations introducing submitted Abstracts, RM 375 Projector available (bring file on usb)
12:00-12:30	Lunch, Room 526 Foyer
12:30-14:25	Student poster session and research discussions, Rm 526 (530, 355, 361 and 375)
14:30-17:00	Tea and Coffee available, Room 526 Foyer
14:30-16:50	Parallel Sessions, Workshop 1 and 2.
Workshop 1	**PDRAs and PhD Students: Sustainable Integrated Renewable Energy Systems for the Future,** Room 526 (355 and 375 available)
14:30-14:50	Introduction to the Workshop, Dr Ian Watson, University of Glasgow; Professor Kunio Yoshikawa, Tokyo Tech

Outline: The costs of renewable energy from solar and wind power is reducing rapidly. This is drastically altering the energy landscape; the growing uptake of these technologies will significantly influence future, global energy scenarios and provide opportunities for developing new technologies. Working in groups, this session will address the role of integrated renewable energy systems for urban and rural deployment and investigate how a country's energy needs and future development of technologies will be met in the future with zero carbon emissions. The groups will develop a strategy to develop methodologies to achieve zero global CO2 emissions and identify the impact of emerging technologies on reducing emissions. Questions that need addressing may include: how does the world reach a position of zero carbon emissions and what problems need addressing and solving to reach this

position? What is the dependency of a country's current political and economic status on reducing their carbon emissions and how will this influence climate change?

Each group will prepare a 10-15 min presentation and two-five pages, referenced synopsis of their work, with time available on Friday to conclude this work from 12:00-13.30. The presentations will be given on Friday from 13:30 and the work combined into a joint document.

Workshop 2 Faculty Round-table workshops: Room 530 (361 available)

Round Table Introductions

14:30-14:55 Faculty Introductions from Japan, 4 mins per institution

14:55-15:05 Professor Trevor Hoey, Dean for University of Glasgow Singapore, "Internationalisation Experiences at the University of Glasgow"

15:05-15:10 Specially Appointed Professor Akinori Nishihara, Tokyo Tech, "TAIST-Tokyo Tech: Transnational Graduate Program in Thailand

15:10-15:20 Professor Jeffrey Cross, Tokyo Tech, **"**Assessing Competencies of Mechanical Engineering students in Japan and Indonesia"

Two to three groups will consider:

1) Transnational Education (TNE) in Engineering and Internationalisation for students and faculty staff;
2) Educating engineering students in interdisciplinary degree programmes and
3) Assessing Competencies of Mechanical Engineering students.
4) Educating engineering students in interdisciplinary degree

The aims of workshop 2 are to identify and develop best practices for developing TNE, research collaborations and educating students in interdisciplinary degree programmes. Can methodologies be developed that fit all countries and what framework would these methodologies take? How would this benefit participating countries and impact delivery of degree programmes, assessing competencies and collaborative research? Specifically, how can the UK and Japanese education sectors work more closely together and what benefits would this yield? The results from each group will be brought together and a presentation produced, for 14:30 on Friday.

17:00 Session Close

18:00-19:30 Evening Reception, Baffo Pizza and Birra, 1377 Argyle St, Glasgow, G3 8AF
Tel: 0141 583 0000

September 8 Friday

9:30-10:00 Coffee/Tea, Room 526 Foyer

10:00-11:00 Lecture by Guest Speaker, Brian Toll, Rm 375
Senior Expert, Europe-Asia Co-operation in Higher Education

11:00-12:00 Joint morning session. Collaborative Research Opportunities and Funding Sources, Rm 375

Brian Toll, Senior Expert, Europe Asia cooperation in Higher Education

Stephen-Mark Williams, CEO, Energy Technology Partnership

12:00-13:30 Working Lunch, Room 526 Foyer
Workshop 1 and 2: Conclude Preparation of Presentations and Documents (355, 361, 375 available)
UKJEEL Business Meeting for Academic Members, Room 530.

13:30-14:30 Workshop 1: Student Presentation and Discussions, Room 375

14:30-15:30 Workshop 2: Faculty Presentation and Discussions, Room 375

15:30-16:00 Coffee/Tea, Room 526 Foyer

15:30-16:25 Joint Wrap up session and prizes: Abstracts, Workshops, Discussions, Rm 375
Joint Collaborative Lessons Learned, Professor Jeffrey Cross, Dr Ian Watson

16:25-16:30 Assoc. Professor James Cannon, Kyushu University, 2018, UKJEEL Workshop Plan, Rm 375

1700 **UKJEEL Close.** Dr Ian Watson and Dean Kikuo Kishimoto, Tokyo Tech, Rm 375

17:30-19:30 Reception, Ubiquitous Chip, 12 Ashton Lane, Glasgow, G12 8SJ
Tel: 0141 334 5007.

TOUR TO LOCH LOMOND ONLY FOR THOSE REGISTERED

September 9 Saturday

09:00-20:00	Coach trip to Loch Lomond and a distillery tour Departure point Memorial Gate, University of Glasgow
09:00-10:30	Travel to Loch Lomond Shores, via Helensburgh
10:30-11:45	Loch Lomond Shores, shopping
11:45:12:00	Travel to Kilted Skirlie, restaurant for lunch Loch Lomond Shores, Ben Lomond Way, Balloch, Alexandria G83 8QL Tel: 01389 754759
12:00-13:15	Lunch at Kilted Skirlie
12:15-14:00	Travel to Glengoyne Distillery, Dumgoyne, Near Killearn, Glasgow, G63 9LB Tel: 01360 550 254 – contacts Helen, Anna.
14:00-14:20	Arrive at Glengoyne Distillery, check-in for tour.
14:20-16:15	Glengoyne Distillery – tour commences at 14:20 (45 mins).
16:30-17:15	Return travel to Glasgow
17:15	Drop off at Mini Grill, 244 Bath Street, Glasgow, G2 4JW Tel: 0141 332 2732
17:45-19:15	Evening Reception, Mini Grill

September 10 Sunday

Japanese students and faculty depart from Glasgow

4. Abstracts

Brian Toll, "Europe, Japan, Glasgow"
Friday 8th, 11am,

Europe: historically important, economically powerful, politically ambitious and academically and in research at the forefront – but the economic model is under pressure. Budgets have been cut in recent - for the first time since the 1950ies - in almost every domain but more attention and more money is increasingly being turned towards education, youth, research and innovation. This follows from the 2010 European Union [EU] blueprint for a bright and stable future: the Europe 2020 strategy, with its specific focus, inter alia, on climate change and renewable energy. But politics has moved on too and the UK has set sail for a 'BREXIT' horizon. And while Japan has not-dissimilar policies to Europe, there are nuances to consider. What will the future offer those of us here today?

The EU has political ambitions outside this framework too, focused on 'strategic partners;' Japan is one of the 10. Why? 'Partner' requires a basis of significant mutual interest… similarities of approach, common values and aspirations in a globalized world where friends count if we are to ensure a 'level playing field' and others can contribute provided they observe common rules (WTO, ILO, etc); the wider 2030 Agenda for Sustainable Development adds another dimension, including the aim of inclusive and equitable quality education and promoting lifelong learning opportunities for all.

In May 2016, Japan hosted the G7 Education Ministers for discussions of current and future challenges facing education systems. What could be done collectively with the tools and policies in place and what new ways of working together could be found? Their conclusions were important and are relevant today: basic skills were seen as lacking in science, technology, engineering and mathematics but a need for balanced for creativity which can be provided by humanities, social sciences, art and design; transversal skills too (e.g. tolerance, confidence, problem-solving ability, critical thinking and curiosity: skills which 92% of employers look for), so that young people can find fulfilling jobs and become engaged, confident citizens.

Since then too, the 'PISA 2015' study results have been published, giving additional emphasis to science, technology, engineering and mathematics in systems producing declining education standards.

In an increasingly complex and digitalised world, learning does not stop with formal education – it continues throughout people's lives. Using Massive Open Online Courses (MOOCs) effectively is a priority for the next ASEM Education Ministerial meeting in November (ASEM includes all EU countries and Japan, 20 other Asian partners and 2 European states, as well as the EU itself and the ASEAN Secretariat, covering around 60% of the world population, GDP and trade and operating on the principle of equal partnership, mutual respect through informal dialogue and tangible cooperation). The view is that modern education and training systems are not currently providing the digital skills and competences to allow people to take part in social, economic and civic life.

This presentation will suggest opportunities for Europe, Japan and, indeed, Glasgow – universities, researchers, staff and students, in particular - through programmes, projects and contacts to promote innovation and global positioning, building on the best of our respective traditions and cultures. Complementing Japan's Top Global University programme, following on from previous efforts to propel

Japan into the highest leagues of university rankings and welcoming foreign students to top-quality higher education in English, these include the EU Erasmus+ programme, aiming to boost skills and employability, as well as modernising education, training, and youth work, supporting 'grassroots' sports projects and cross-border challenges such as match-fixing, doping, violence and racism; the Marie Skłodowska-Curie actions, funded under the "Excellent Science" pillar of the Horizon 2020 research programme, support the career development and training of researchers – with a focus on innovation skills – in all scientific disciplines through worldwide and cross-sector mobility.

Optimization of a 1m^3 PBR: A focus on the light distribution and culture-agitation

Allen Akwu-Ude, Kelvin Egbo, Holly Macdonald, Rowan Blaney, Ian Watson
Systems, Power & Energy Research Division, University of Glasgow
e-mail: a.akwu-ude.1@research@gla.ac.uk, ian.watson@glasgow.ac.uk

Keywords: Photosynthetic Photon Flux Densities (PPFD), biofuels, biodiesel, microalgae, photobioreactor (PBR)

I. ABSTRACT

The work focused on optimizing the lighting properties within a Photobioreactor (PBR) by strategic placement of LEDs with the aim of reducing dark zones within a 1 m3 cube-shaped PBR. MATLAB simulation results for two LED sets with different PPFDs were compared alongside distributions within the PBR. Flow simulation results illustrated the flow patterns and velocity distributions based on the positioning of the air diffusers. ANSYS Fluent simulation showed that the fluid velocity is maximum (1.079 ms^{-1}) along the vertical walls adjacent to the diffusers and at the middle of the PBR when the air inlet velocity of was 0.025 ms^{-1}.

II. INTRODUCTION

Microalgae, being unicellular microorganisms thrive under suitable lighting, nutrient and cell densities and contribute in the direct capture of CO_2 from the atmosphere. They play a vital role in the mitigation of the impacts of greenhouse gases generated from the combustion of fossil fuels and require the development of large scale and sustainable growth systems (PBRs). Large PBRs require adequate lighting (quantity and quality) and agitation (mixing) for optimized microalgae growth; these are key parameters to be considered when designing these systems.

III. METHODOLOGY

9 clear hollow tubes,1m long with internal diameter of 26mm and external diameter of 30mm each are assembled as shown in Figure to serve as the LED housing for the PBR. 5 x 2.5W LEDs are arranged in series within each of the tubes as shown in Figure 2.

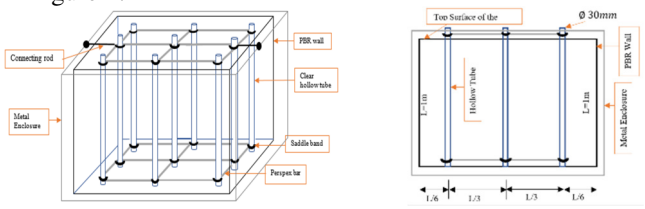

Figure 1 (a) Isometric view (b) Lateral view of the LED compartments

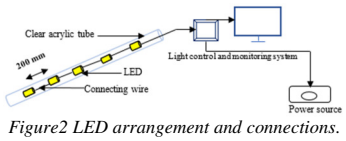

Figure2 LED arrangement and connections.

Light attenuation in a medium due to a point light source is based on Beer-Lambert law. This law defines the absorbance A of a medium with respect to its transmittance $\frac{I}{I_o}$ (Eq. 1). Equation 1 can also be written in terms of the properties of the medium (concentration c, distance of the light-path L, and the molar absorptivity which is dependent on the wavelength of the light σ) (Eq. 2)

$$A = \log_{10}\frac{I_o}{I} \quad (1), \qquad A = \sigma LC \quad (2),$$

From Eq. 1 and Eq. 2 it can be shown that

$$I = I_o e^{-\sigma Lc} \qquad (3)$$

IV. RESULTS

Figure 33 shows the modelled light distrbutions within the PBR based on the proposed light source arrangement. The light sources in each setup has a different PPFD.

Figure 3 (a) A 2D MATLAB representation of the light distribution within the PBR with a max PPFD of 160 µmol m^{-2} s^{-1} (b) A 2D MATLAB display of the light distribution in the PBR with a max PPFD of 140 µmol m^{-2} s^{-1}.

V. AGITATION (MIXING)

High-cell-density microalgal cultures could be as high as 10^9 cells/mL which may result in drastically reduced transmission of light and increased rates of CO_2 consumption and DO accumulation, as well as quick increase of culture temperature. Mixing prevents biomass sedimentation and ensures uniform average exposure to light and nutrients. It also facilitates heat transfer and helps avoid thermal stratification and improves gas exchange within the culture medium (Wang, , 2012). Figure 14 (a) shows the design and positioning of the diffusers within the PBR. This was supported by flow simulations (ANSYS Fluent CFD and laboratory experiments) (Figure 14 (b)).

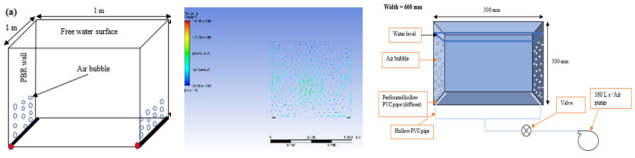

Figure 1 (a) Diffuser positioning within the PBR (b) Contour image of the velocity distribution within the PBR (c) Experimental setup for the bubble flow.

VI. CONCLUSION

The optimization of microalgal cell growth and biomass production within a 1m3 PBR is dependent on adequate lighting and light distribution with the PBR and adequate mixing/aeration ensuring a homogeneous mix and adequate gas exchange.

VI. REFERENCE(S)

Wang, B., Lan, C.Q. & Horsman, M. (2012) Closed photobioreactors for production of microalgal biomasses. *Biotechnology Advances*. [Online]. 30 (4) pp.904–912. Available from: doi:10.1016/j.biotechadv.2012.01.019.

Modelling and Analysis of Wind Energy Systems and Hydropower Plants for Remote Areas

Anas Shoaib, Ian Watson
School of Engineering, University of Glasgow, UK.
e-mail: anas.shoaib@gmail.com

Keywords: Wind, Hydro, Renewable, Modelling, MATLAB

I. ABSTRACT

Renewable energy is the energy obtained from renewable and resources that are naturally. Wind and hydro are widely used renewable energy technologies. Wind turbines can vary in size and power and are generally designed to operate in optimum conditions. In the present case a coupled model of wind turbines and hydropower plants was produced. The impact of variable wind speeds, through different temporal domains, passed through a 1.5MW wind turbine on the turbine's output was assessed. A synchronous generator was used in this system as it eliminates the gearbox. The model also assessed variation in load requirements. The hydropower plant was modelled as a run-of-river system. An electrical storage model was developed to integrate the wind energy and hydropower plants to provide non-intermittent renewable energy solutions for remote regions. Electrical energy storage of 0.5 MW was assumed. These two individual systems provide an opportunity for electrical energy storage, allowing efficient power delivery on demand through the day and night. These systems are modelled and simulated in MATLAB / Simulink.

II. METHODOLOGY

A. Equations

Generated power provides data about how much load a wind turbine can bear and whether sufficient torque is generated to drive the permanent magnet synchronous generator (PMSG). Both of these are modelled by using the following equations: [1]

$$P = \frac{1}{2} C_p(\lambda, \beta) \rho \, A \, v^3 \quad (1)$$

$$T = \frac{P}{\omega} \quad (2)$$

Where P is power, T is torque, Cp is performance coefficient, ρ is density, A is the area covered by the rotor blade, ω is rotor speed and v is the wind speed.

Three-phase power is generated by the generator which passes through the full-scale converter which can be used to supply the load.

Hydropower depends upon mechanical power, pressure head and water flow. Head remains constant whereas flow changes according to how much the gate is opened and how much power is needed. Equations used to model the hydropower system are given below: [2]

$$Pm = H * U \quad (3)$$

$$H = \left(\frac{U}{g_{max} - g_{min}}\right)^2 \quad (4)$$

$$U = \frac{H_o - H}{T_w s} \quad (5)$$

Where U is flow of water, H_o is initial head, H is net head, Tw is time constant, g_{max} and g_{min} are highest and lowest positions of the gate. Reference power specifies how much mechanical power a turbine can generate. A P_{ref} of 1 specifies full mechanical power, 0.5 specifies half mechanical power and 0 specifies no mechanical power. The model was integrated with a Solar PV model.

III. CONCLUSION

The wind turbine did not generate torque for wind speeds less than 4 m/s; for speeds greater than 20 m/s, no power was generated as the turbines are disabled. Stator currents, rotor speed and torque were observed from the generator. Three-phase power was generated at 60Hz by the full-scale converter which was then given to the load. The hydropower plant reacts to different reference powers, and to changes in the flow and gate accordingly whereas the head remains constant. The state of charge showed switching of systems for different conditions. This standalone system will be able to supply an average energy of 4700 kWh per year to 7500 homes in remote areas. Moreover, the energy density of the integrated system is 4 W/m2 which is good as it includes solar which takes a large amount of area. The total generation capacity of the system is 4 MW (1.5 MW Wind, 1 MW Hydro, 1 MW Solar PV and 500 kW Energy Storage).

REFERENCES

[1] Modeling and Control of a Variable-Speed Wind Turbine Equipped with Permanent Magnet Synchronous Generator, D.C. Aliprantis, S.A. Papathanassiou, 2009.

[2] Simulation and modeling of hydro power plant to study time response during different gate states. Chauhan, G. Singh, 201

Non-destructive Inspection for CFRP Component with Corner Shape

Takeshi ASHIZAWA*, Yoshihito MIZUTANI*, Akira TODOROKI* and Yoshiro SUZUKI*
*Department of Mechanical Engineering, Tokyo Institute of Technology, Japan
e-mail: tashizaw@ginza.mes.titech.ac.jp

Keywords: CFRP, Composite material, Non-destructive inspection, Ultrasonic wave

I. INTRODUCTION

A. CFRP

Carbon fiber reinforced plastics (CFRP) is a kind of composite material, which consists of carbon fibers and polymer such as nylon or epoxy. In other words, CFRP is plastics which contain carbon fibers in. Due to carbon fibers, CFRP has high specific strength and high stiffness, thus CFRP are often used in various engineering field such as aerospace industry, automotive industry and so on.

Figure 1 shows the schematic image of CFRP. Since CFRP have fiber direction and transverse direction, CFRP is anisotropic materials of which material properties depends on directions to the fiber direction. Due to anisotropy, the propagation behavior of ultrasonic also has anisotropy.

B. Non-destructive inspection

When inner defects are generated in CFRP, it is necessary to conduct non-destructive inspection. Ultrasonic testing method is one of the general non-destructive inspection methods.

Figure 2 shows the schematic image of Ultrasonic testing for CFRP. By using probe, ultrasonic wave was emitted from the probe and echo from defect is measured.

II. ULTRASONIC BEHAVIOR ON CFRP

As shown in Fig.3, when CFRP has straight fibers, ultrasonic wave propagate along the fiber direction [1] [2]. However, the propagation behavior of ultrasonic wave has not elucidated yet. It is considered that the behavior of ultrasonic is highly complex. Due to this character of curved fiber CFRP, it is difficult to detect defect on the corner area of CFRP which has curved fibers. In this research, the propagation behavior of ultrasonic wave is studied in order to consider the method to detect defects on the corner of CFRP with curved fibers.

III. NUMERICAL SIMULATION

Numerical simulation is one of the effective methods to clear the propagation behavior of ultrasonic wave on curved fibers. In this research, simulation program was implemented by using finite difference method.

Figure 4 shows the result of numerical simulation of ultrasonic wave. In Fig.4, upper side of figure shows propagation of ultrasonic wave in aluminum which is isotropic material. It is observed that ultrasonic wave propagate straight to the horizontal direction.

On the other hand, in lower side of Fig.4, propagation of ultrasonic wave in CFRP which has curved fibers is shown. It is observed that ultrasonic wave curve along curved fibers.

IV. CONCLUSION

It is confirmed that the behavior of ultrasonic wave propagation in CFRP with curved fibers is quite different with an isotropic material such as aluminum. In addition, ultrasonic waves curve in CFRP with curved fibers.

REFERENCES

[1] B. A. Auld, Acoustic Fields and Waves in Solids Volume I, 2nd, Krieger (1990)
[2] Joseph L. Rose, Ultrasonic Guided Waves in Solid Media, Cambridge University Press (2014)

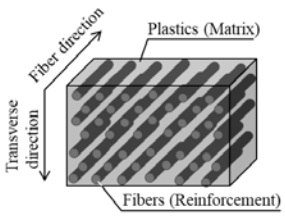

Fig.1 The schematic image of CFRP.

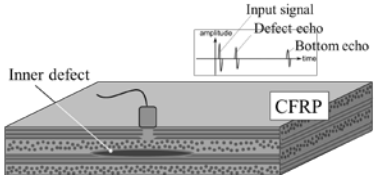

Fig.2 Ultrasonic testing for CFRP.

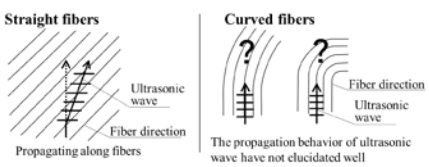

Fig.3 Ultrasonic wave in CFRP with straight fibers and curved fibers.

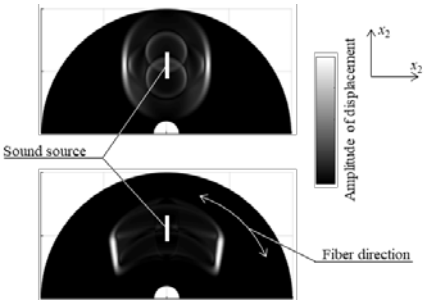

Fig.4 Numerical simulation of ultrasonic wave in Aluminum (upper) and CFRP with curved fibers (lower).

Kinetic investigation on thermal tar cracking during biomass gasification process

D.A. Buentello Montoya*, X. Zhang* & S.P. Marques*
*School of Mechanical and Aerospace Engineering, Queen's University Belfast, United Kingdom
e-mail: xiaolei.zhang@qub.ac.uk

Keywords: Tar, cracking, openfoam, kinetics, kriging

I. INTRODUCTION

The presence of tars within the biomass gasification process will damage the downstream equipment, therefore it is a critical issue to be addressed. Different tar removal strategies have been proposed, namely chemical, physical and thermal technologies. For industrial scale applications, chemical and physical processes are complicated since they either need the utilisation of catalysts or produce waste, whereas thermal technologies have shown promise without these shortcomings. Nevertheless thermal degradation is constrained by the necessity of high temperatures, limiting its applicability. Further development is needed for its industrial scale usage. In order to better comprehend the relationship between thermophysical parameters and tar degradation, thermal cracking of selected tar compounds (naphthalene, toluene and benzene) was investigated adopting CFD (OpenFOAM).

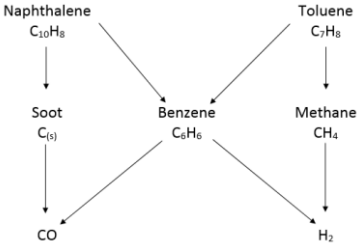

Figure 1. Tar model compounds and simplified chemical pathways.

II. METHODOLOGY

A 2D tubular reactor with heated walls was considered to model the tar cracking process. The modelling results were validated by comparing with the experimental results

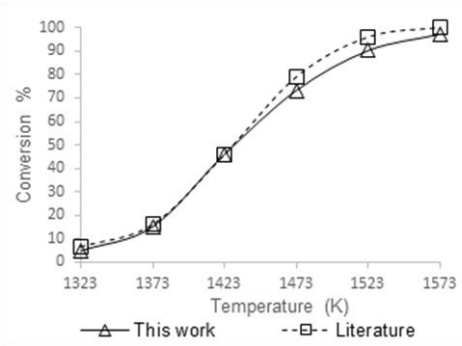

Figure 2. Comparison of naphthalene conversion under a range of temperatures, 0.5 seconds residence time with reference [1].

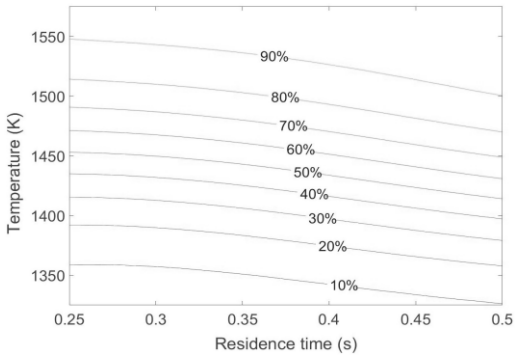

Figure 3. Naphthalene conversion percentage as a function of temperature and residence time

reported in literature [1]. Selection of the model compounds of tar was made based on their presence in tar lumps, stability and overall significance in reaction pathways. Since sophisticated reaction kinetics are computationally expensive, a global mechanism was used within this work. As chemical kinetic modelling is based on numerical correlations that describe observed phenomena, room for improvement lies in determining the most important factors in reaction pathways. Plots describing compound conversion under a range of temperatures and residence times are presented. Sensitivity analyses for temperature and residence time time (1273-1573K and 0.25 – 0.5s) show a higher dependence on temperature compared to residence time, with effects increasing with temperature. Surfaces were obtained using a kriging response surface [2] to estimate the conversion for different values of temperature and residence time. Results indicate that for example, over 90% naphthalene can be converted at 1550K with residence times as short as 0.25 seconds. Furthermore, the effect of temperature is more pronounced for the cracking of benzene, rather than that of naphthalene and toluene, indicating its importance in the overall reaction mechanism. Therefore, as determined by sensitivities and conversion, benzene reactions are the rate defining step in the overall model compound cracking mechanism.

Future work will incorporate a more realistic kinetic as well as further analysis on the sensitivies from the respective surrogate model.

REFERENCES

[1] A. Jess, "Mechanisms and kinetics of thermal reactions of aromatic hydrocarbons from pyrolysis of solid fuels", Fuel, vol. 15, pp. 1441-1448, 1996.

[2] S.N. Lophaven; H.B. Nielsen; J. Søndergaard, "DACE, A MATLAB Kriging Toolbox", Informatics and Mathematical Modelling, Technical Report IMM-TR-2002-1

Multiphysics Simulation of Thermal Plasma for Lightning Strike Modelling

J. Campbell*, G. Abdelal, Y. Mahmoudi, A. Murphy, B. Falzon
*School of Mechanical and Aerospace Engineering, Queen's University Belfast, United Kingdom
e-mail: jcampbell2002@qub.ac.uk

Keywords: lightning, simulation, plama

I. INTRODUCTION

It is recorded that an aircraft will experience a lightning strike event approximately once in every 3000 hours of flight time, corresponding to a strike each year for most commercial aircraft [1]. The use of epoxy/carbon fiber reinforced polymer (CFRP) composite materials has become prevalent in aerospace engineering due to the decreased weight resulting in higher fuel efficiencies. These composites, however, are particularly vulnerable to damage induced by lightning strikes. Current solutions see metallic meshes or paints adhered to the surface to increase the electrical conductivity [2], however this adds parasitic weight without serving any other structural purpose. Current state of the art integrates carbon nanotube (CNT) assemblies with epoxy/CFRP composites as a means of increasing the electrical conductivity of the panel thus increasing the lightning strike protection, as well as enhancing the mechanical performance [3][4].

With the vast number of possible assemblies, optimising the nano-enhanced composite configuration with respect to lightning strike protection is both time and resource intensive and often results in destructive testing. A numerical model is in development to assist this optimisation procedure by modelling the physics of a lightning strike and its interaction with a composite surface in order to help researchers tune design parameters based on the predicted response, saving both time and resources.

Lightning strikes are characteristically very high energy phenomena, with temperatures exceeding 20,000 K in a very short time period (< 500 μs). In order to replicate these conditions in a laboratory for material testing, the phenomena is broken into characteristic behaviours, termed "waveforms"[5]. The simulations presented here will replicate the conditions associated with these waveforms in order to compare with physical results obtained through these experiments.

II. METHODOLOGY

A numerical model was created in COMSOL Multiphysics utilising finite element method (FEM) to solve the magnetohydrodynamics (MHD) equations for a characteristic waveform-B lightning strike event. Similitude theory was used to scale the problem in order to reduce the severe computational cost of the complex simulation. This approach can estimate values of current flux, temperature, and velocity and pressure profiles in less than 10 days. Across the 5 μs simulation, peak temperatures of 40,000 K and pressures ranging 0.1-0.2 MPa were predicted while the surface temperature remained in the range of 300K due to the short duration of the lightning strike event. The low surface temperature and pressures calculated suggest that pressure loading through waveform-B has a minimal effect on composite material damage. Future models will include air plasma chemical composition and detailed plasma-surface interactions.

The next stage of research is underway to simulate this test case using OpenFOAM, an open-source software based in C++ that uses finite volume method (FVM) to solve partial differential equations (PDEs). Through OpenFOAM, solvers can be freely edited or custom built from the ground up to solve specific problems allowing the user full control over the equations to be solved in a way that's computationally inexpensive. This is in contrast to commercial software where heavy licences restrict the installation on high performance computing facilities and the PDEs to be solved are inaccessible, essentially acting as a "black box".

Through OpenFOAM, three solver modules are built to simulate the fluid dynamics, the heat transfer between fluid and surface and the electromagnetic behaviour of the plasma channel respectively before being combined to form a single complete plasma physics solver that includes temperature dependent plasma properties.

REFERENCES

[1] M. A. Uman and V. A. Rakov, "The Interaction of Lightning with Airborne Vehicles," vol. 39, pp. 61-81, 2003.

[2] M. Gagné and D. Therriault, "Lightning Strike Protection of Composites," *Prog. Aerosp. Sci*., vol. 64, pp. 1-16, 2014.

[3] T. Subhani et al., "Mechanical Performance of Epoxy Matrix Hybrid Nanocomposites Containing Carbon Nanotubes and Nanodiamonds," *Mater. Des.*, vol 87, pp. 436-444, 2015.

[4] H. Mei et al, "Dramatic Increase in Electrical Conductivity in Epoxy Composites with Uni-directionally Oriented Laminae of Carbon Nanotubes," *Chem, Eng. J*., vol. 304, pp. 970-976, 2016.

[5] "Aircraft Lightning Environment and Related Test Waveforms Standard," *Aerospace Reccomended Practice ARP5412*, SAE, 1999.

Development of a portable ultra-small biomass gasification and power generation system

Xin Dai*, Kunio Yoshikawa, Lu Ding, Muhan Li, Minoru Fukuhara
Department of Transdisciplinary Science and Engineering, Tokyo Institute of Technology, Japan
E-mail: dai.x.aa@m.titech.ac.jp

Keywords: biomass gasification; power generation; portable; briquette; carbonization

Syngas from biomass gasification is a kind of sustainable energy that can be used for electricity power generation. There is a huge demand for a portable small scale biomass gasification and power generation system in the disaster areas or un-electrified rural areas of developing countries.

Carbonization was used to deal with the high moisture and inhomogeneity property of biomass resources[1]. After carbonization, volatile matter in the feedstock decreased and the percentage of carbon increased. A ball press machine(240-type, China) was used for the densification. Gasification was achieved by an up-draft gasifier. Tar content in the syngas was reduced by several cleaning devices including a water scrubber, an oil-scrubber, a char bed and a bag filter. The KLD-6110 type gas engine was adopted for electricity power generation. The schematic diagram of the whole system is shown in Figure 1.

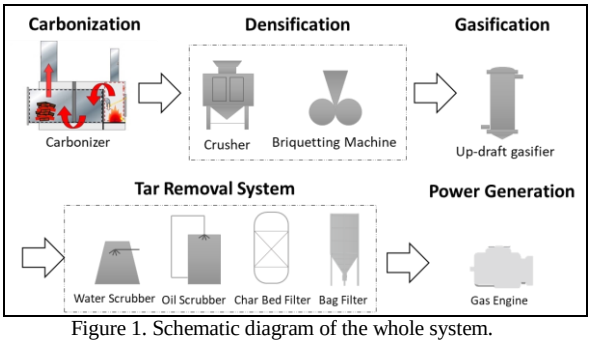

Figure 1. Schematic diagram of the whole system.

By increasing the carbonization temperature, the high heating value of char increased and the volatile mater residue in char decreased (Table I). Finally, the carbonization temperature was fixed at 400 ºC.

Table I. Chemical composition of carbonized wood.

	Proximate Analysis, wt.%			Ultimate Analysis, wt.%				LHV[c], MJ kg^{-1}
	VM[a]	FC[b]	Ash	C	H	N	O	
Cedar Wood	84.59	11.42	3.99	36.08	4.43	0.11	59.38	18.8
Char/400 ℃	43.9	53.5	2.6	80.48	2.69	1.11	15.72	31.6
Char/450 ℃	36.1	62.8	1.1	81.68	3.18	0.43	14.71	32.52
Char/500℃	33	65.2	1.8	85.46	2.49	0.23	11.82	33.5

a: Volatile Matter, b: Fix Carbon, c: Lower Heating Value

In order to increase the quality of briquette, corn starch solution (9.1 wt.%) was used as a binder. After drying, the briquette was used for gasification. After 3 h operation, the gasification system became stable when the syngas production rate increased to 70 m^3/h and the CO concentration in the syngas increased to 27%. The calculated lower heating value of the syngas was 4.63 MJ/m^3[2]. The composition of the syngas during the gasification was shown in Figure 2.

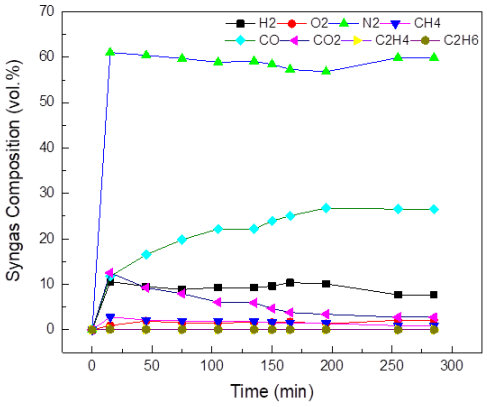

Figure 2. Composition of the syngas during the gasification.

Tar content in the syngas was reduced by the tar removal system. The tar concentration in the syngas decreased from 4.30 g/m^3 to 0.26 g/m^3 (the tar concentrations after the gasifier and before the gas engine, respectively)[3]. During the stable stage of the gasification, the power output of the gas engine was 25 kW which was determined by a load testing. The thermal efficiency of the gas engine was 27.79%.

Biomass is a kind of renewable, available energy. Especially for meeting the energy or power demands from disaster places or remote areas. A potable biomass gasification and power generation system was established. Biomass gasification was achieved by the carbonization, the densification and the gasification. Tar content in the syngas was reduced by a secondary tar cleaning system. Finally, a stable 25 kW power generation was achieved by a gas engine.

References

[1] Nanou, P.; Carbo, M. C.; Kiel, J. H. A., Detailed mapping of the mass and energy balance of a continuous biomass torrefaction plant. *Biomass and Bioenergy*, 89, 67-77, 2016.

[2] Couhert, C.; Salvador, S.; Commandré, J. M., Impact of torrefaction on syngas production from wood. *Fuel*, 88 (11), 2286-2290, 2009.

[3] Nakamura, S.; Kitano, S.; Yoshikawa, K., Biomass gasification process with the tar removal technologies utilizing bio-oil scrubber and char bed. *Applied Energy*, 170, 186-192, 2016.

Black Liquor Utilization for Electricity Production: an Enhanced Integrated System

Arif Darmawan* Flabianus Hardi, Kunio Yoshikawa, Muhammad Aziz, Koji Tokimatsu
*Department of Transdisciplinary Science and Engineering, Tokyo Institute of Technology, Japan
e-mail: arifdarmawan33@gmail.com

Keywords: black liquor; evaporation; gasification; exergy recovery; energy efficiency; power generation

I. INTRODUCTION

Energy recovery from black liquor (BL) can be performed through gasification at temperatures above the melting point of inorganic chemicals. Complementarily to BL gasification experimental research, this study is conducted to simulate the thermodynamic modeling of an integrated system for BL evaporation, gasification, and combined cycle for power generation. We propose a scheme for energy-efficient evaporation of BL based on the concept of exergy recovery. The effect of target solid content on the energy required for evaporation is evaluated. In addition, an integrated gasification and combined cycle based on process integration is modeled and the net energy efficiency of the integrated system is calculated. [1]

II. PROCESS MODELING AND CALCULATION

The flow rate of weak BL entering the evaporation module is 348.12 t h^{-1} (considering pulp production of 730 t d^{-1}). Material composition is shown in Table 1.

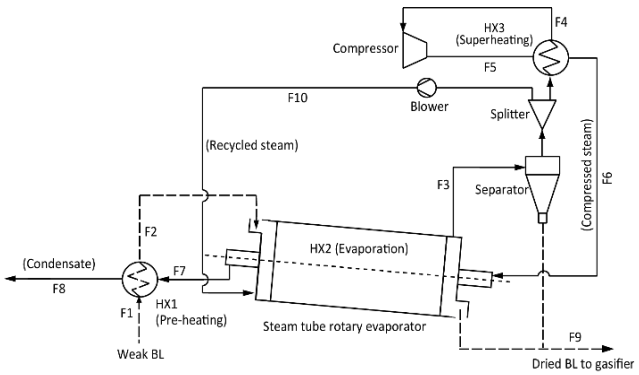

Figure 1. Arrangements and process flow diagram of proposed BL evaporation

TABLE I.
MATERIAL COMPOSITION OF BL

Properties	Value
Total solids (wt% wb)	15
Water content (wt% wb)	85
Components (wt% db) [2]	C: 27.50; H: 3.75; O: 39.35; N: 0.07; Cl: 0.16; Na: 19.85; K: 3.12, S: 6.20
LHV (MJ kg^{-1}, db)	12.13

Figure 2 shows the process flow diagram of the proposed integrated-system for power generation covering the gasification and combined cycle processes.

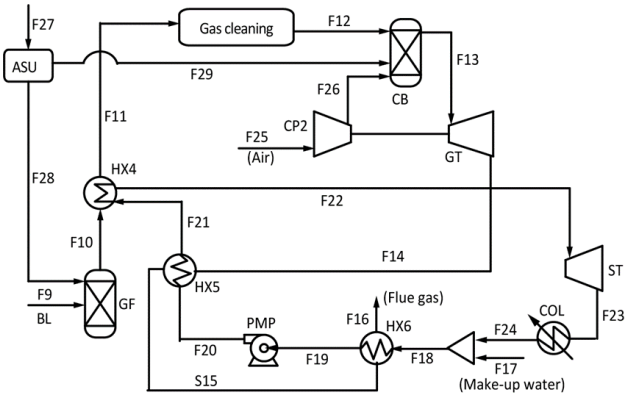

Figure 2. Proposed process flow diagram covering BL gasification and combined cycle

III. RESULTS AND DISCUSSION

In this case, the target moisture content in the evaporation process is fixed at 22.5 wt% wb (target solids content of 77.5 wt% wb). From the simulation, the required total energy input (work), Wtot, is 8.1 MW, comprising compressor and blower duties of 7.61 MW and 0.49 MW, respectively. In addition, the outlet steam pressure and temperature of the compressor are 155 kPa and 167 °C, respectively.

The result shows, gas turbine compressor consumes the highest energy followed by the evaporation and ASU. The net generated power from the integrated system is about 60 MW (pulp production of 730 t d^{-1}). Compared to the most recent BL gasification and combined cycle system studied, the proposed integrated system can double the net energy efficiency, 18% compared to 34.5%. This is significantly higher than adoption of multi-effect evaporators (24.5%) and conventional boiler-based evaporation (14.7%).

REFERENCES

[1] Darmawan et al. Enhanced process integration of black liquor evaporation, gasification, and combined cycle. Appl Energy (2017), http://dx.doi.org/10.1016/j.apenergy.2017.05.058

[2] Jafri Y, Furusjö E, Kirtania K, Gebart R. Performance of an entrained-flow black liquor gasifier. Energy Fuels 30 (2016) 3175–3185.

Gasification of Scottish Agricultural Waste

H.S.Dhami* and M.C.Paul*
*Systems, Power & Energy Research Division, School of Engineering, University of Glasgow, UK
e-mail: harry.dhami@glasgow.ac.uk

Keywords: Scottish, Agricultural, Waste, Gasification & CHP

I. INTRODUCTION

Gasification of biomass is playing a key role in reducing greenhouse gas emissions worldwide. In 2013, the supply of bioenergy was 57.7 EJ – 10% of the global energy supply [1]. Combining gasification with CHP (combined heat and power) generation gives great potential to produce electrical and thermal power onsite, completely decentralized from the main grid.

A technical model was developed to determine the gasifier dimensions and syngas quality for the University CHP system for Scottish agricultural biomass feedstocks (oat straw, wheat straw, barley straw, rape stalk & sunflower stalk.)

II. METHOD

The model developed is able to determine the physical dimensions of the gasifier required to power any CHP engine for any type of biomass waste. The model also gives a detailed analysis of the producer gas and concentrations. The model allows for analysis of any biomass waste specific to any geographic location in the world. By entering the ultimate analysis of the feedstock and the required thermal and electrical power outputs into the model, the model then generates the optimum gasifier design and predicted syngas quality in addition to the tar content and heating values.

The feedstocks analyzed for the purposes of this research is based on Scottish agricultural waste.

III. RESULTS & DISCUSSION

Figure 1 illustrates the HHV (high heating value) and tar content for all the feedstock analysed. The results show the effects of varying the feedstock on the HHV and tar content produced. It can be seen that wheat straw has the largest HHV. The HHV is dependent on the moisture content of the feedstock. In this case the moisture content of the wheat straw is 5.9%, the lowest moisture content compared to other feedstocks. Feedstock's with a lower moisture content result in higher values of CO and H2, as a result the HHV increases. As the moisture content increases the energy required to remove the moisture is not recoverable and can be seen as lost energy. As a direct result the heating value is lower due to the energy losses which stem from removing moisture. On the contrast barley straw has the lowest HHV due to high moisture content of the feedstock. Furthermore, the tar content produced is highest for barley and lowest for wheat. This is due to the fact that the moisture content is directly related to the amount of tar the system produces. In order to reduce the tar content, the moisture content must be reduced by means of drying the feedstock before gasification. It was reported in [2] that a decreasing the moisture content from 20%-5% results in a decrease of 18-26%.

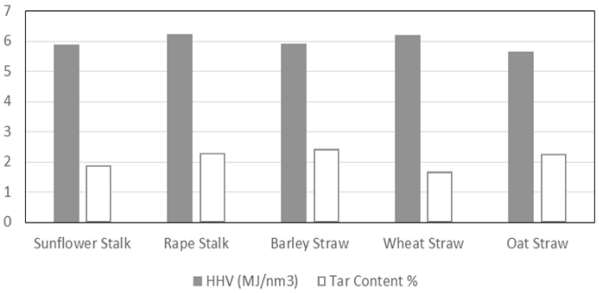

Figure 1. HHV and tar content of tested feedstocks.

Figure 2 illustrates the fuel feed rate of the gasifier for given power outputs of the CHP engine. It can be seen that a gasifier with a wheat straw feedstock would require the least amount of feed in comparison to the other feedstocks. To power an engine at 25% load the gasifier would require 411kg of wheat straw per hour. Wheat straw in this case is the most optimal feedstock due to its properties, it has the highest HHV compared to other feedstocks and thus the engine would require less feedstock in comparison to other feedstock.

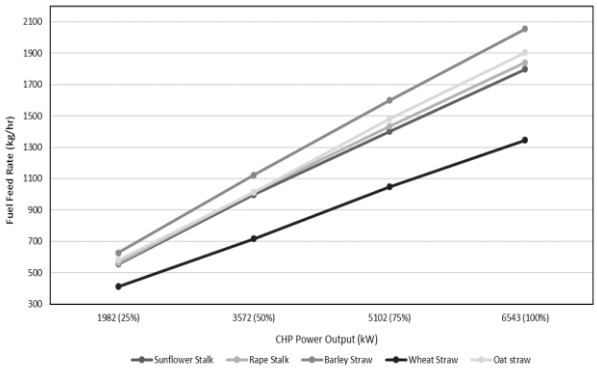

Figure 2. Fuel feed rates required for a 6.5MW CHP engine for varying feedstocks.

REFERENCES

[1] [Online].Available: http://data.worldbank.org/indicator/EG.ELC.LOSS.ZS?end=2014&locations=GB&start=1960&view=chart&year_high_desc=false.

[2] A.M. Salem and M.C. Paul, "An Integrated kinetic model for a downdraft gasifier based on a novel approach," International Journal of Advances in Science Engineering and Technology, vol. 4, no. 3, pp. 182-185, 2016

Analytical Study of Transport and Entropy Generation in Microreactors

G, Hunt*, N. Karimi*, M. Torabi
*School of Engineering, University of Glasgow, UK
e-mail: G.Hunt@research.glasgow.ac.uk

Keywords: Microractors; Combined heat and mass transfer; Mathematical modelling

I. INTRODUCTION

First and second law analyses are conducted to obtain an understanding of the influences of the configurational and operational parameters upon transport phenomena and entropy generation in a microreactor.

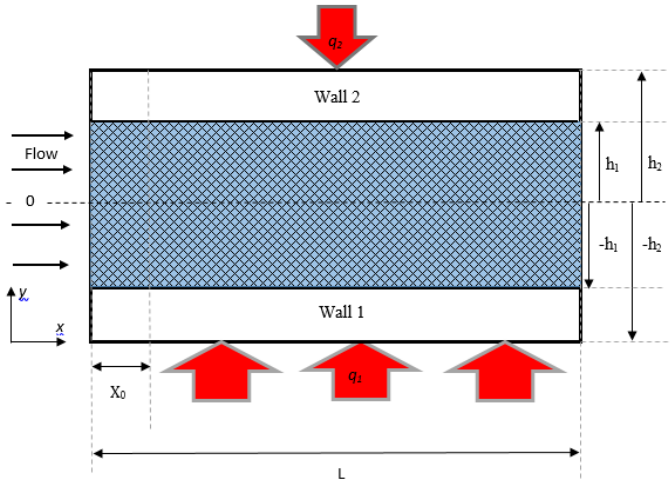

Fig. 1. Schematic of the system under investigation.

Axial evolution of temperature is determined independently from the transversal changes. Using the LTNE model of heat transfer within the porous insert and standard thermal models for the solid walls, a series of linked differential equations are defined to govern the transverse temperature distribution. Analytical solutions of these equations results in the calculation of the temperature fields and the Nusselt number. A similar approach is taken to solve the diffusive-advective equation of mass and the Soret effect is taken into account. The local entropy generation is subsequently evaluated through the knowledge of temperature and concentration fields.

Understanding the influences of the microstructure upon the thermal behaviour of the system is an important objective of this work. To this end, variations in the wall thickness and thermal conductivity serve as indicators. Wall thickness is shown to have significant impacts on the thermal distribution within the porous insert. Thickening of the walls leads to a significant increase in the axial temperature range within the insert in the solid and porous phases. The thermal conductivity of the lower wall makes no change in the range of temperature distribution but strongly affects the actual temperature values within the channel. As expected, increasing the thermal conductivity in the wall increases the temperature of the porous insert for the solid and fluid phases. Interestingly, without varying the total imposed heat flux, a variation in the heat flux ratio (of top wall total) revealed that as the heat flux ratio became less symmetric, the temperature in the channel increased.

II. RESULTS AND DISCUSSION

The local entropy generation for the various aspects of the geometry of the system clearly shows the dominance of the entropy generated by thermal diffusion of mass. This irreversibility was found to be two or three orders of magnitude greater that the other sources of irreversibility. It should be clarified that the neutralisation of Soret effect results in the reduction of mass transfer irreversibility to values similar to those of other irreversibilities. As anticipated, the fluid friction contribution to the local entropy shows the highest value of entropy generation at the boundary between the porous insert and the thick walls. This irreversibility deceases towards the middle of the channel and then increases again, showing a peak in local entropy generation in the middle of the channel. The increased flow velocity in the part of the channel would be most likely responsible for this. Notably as the wall thickness increases, this peak reduces.

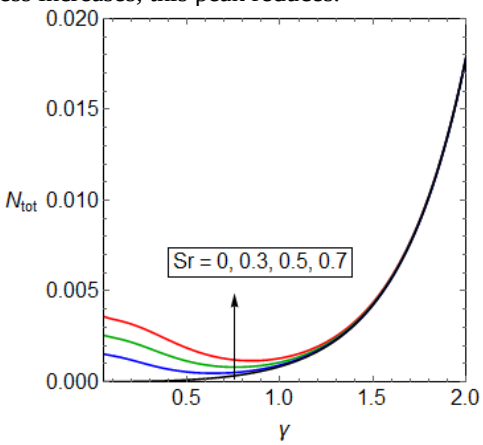

Fig. 2. Total Entropy curves for varying Damköhler number, γ with various values of Soret number, Sr.

Through an analytical approach, this work provides a means of evaluating the influences of microstructure and uneven thermal loads on the temperature and concentration fields in a microreactor. It also demonstrates the significance of Soret effect in the second law performance of microreactors.

In-situ Diagnostics of Damage Accumulation in Nickel-based Superalloy

K. Kageyama[1], F. Adziman[2], T. Sui[2], A. Korsunsky[2] and R. C. Reed[1,2]
[1]Department of Materials, University of Oxford, UK
[2]Deparrment of Engineering Science, University of Oxford, UK
e-mail: koji.kageyama@materials.ox.ac.uk

I. Introduction

Nickel-based superalloys are widely used under harsh environment for critical applications requiring excellent high temperature efficiency, *e.g.* jet engines in aerospace, or gas and steam turbines in energy industries. The high demand is owing to their high performance – notably at elevated temperatures, in terms of strength, creep, and fatigue behaviours. Nevertheless, much effort is still needed to capture, understand, and enhance their fracturing mechanisms at such severe conditions, for which various post-mortem or *ex-situ* analyses of their damaged materials have always been the norm. For instance, *ex-situ* X-ray Computed Tomography (XCT) has been ubiquitously used to detect voids and cracks in nickel-based superalloys[1]. However, *ex-situ* XCT inherently has inevitable limitation in investigating sequence of fractures, in particular at high temperatures – interrupted tests would be needed that may lead to inaccuracy. To circumvent these deficiencies and, in addition, to better understand how cracks or voids affect the material strength, plastic behavior, and fracturing lifetime; in this study, we intend to develop a new *in-situ* XCT system. The new system, which is specifically designed to be used at a wide spectrum of temperatures, is able to detect evolution of cracks and its corresponding effect to the investigated mechanical behaviour of nickel-based superalloys.

II. Methodology

A new *in-situ* XCT setup was developed by integrating it to a dedicated high temperature mechanical testing system. Microfocus X-ray source of Hamamatsu Photonics with the capacity of 150keV and SCMOS X-ray detector of Photonic Science were paired to detect XCT images. During the test, the tensile axis of the mechanical testing system is rotatable whilst maintaining zero torque and fixed positions of the X-ray source and detector. This enables the system to capture multi-angle back projection images for use in the 3D reconstruction. ImageJ[2] was used to reconstruct 3D voxels upon generating sliced images by using the inverse Radon transformation in MATLAB. For the *in-situ* XCT experiments, high temperature tensile experiments were conducted using Nimonic 80A, a commercial polycrystalline Ni-based superalloys. The testing specimens were designed of having a gauge length of 2 mm and 1.5 mm diameter. Temperatures during the tests were set to 25, 200, 600, and 800 degrees C, and strain rates were chosen from 10^{-5} and 10^{-3} /s.

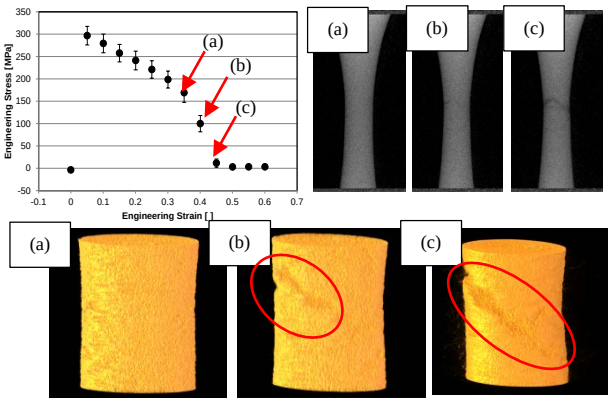

Figure 1. Tensile test reaults (10^{-3}/s, 800ºC) for Nimonic 80A with corresponding XCT projection images.

III. Results and Discussion

Tensile and *in-situ* XCT test results for Nimonic 80A at 800ºC with strain rate of 10^{-3}/s are shown in Figure 1. Captured sequential XCT projection images demonstrate evolution of crack propagation after necking and crack initiations. The latter confirmed the apparent immediate strength softening in the stress-strain curve (the error bar indicates load fluctuations during rotation of tensile axis while capturing projection XCT images). This sample does not display the necking behaviour (Fig. 1(a)). Stress value was notably dropped when a crack initiation was observed on the sample surface (Fig. 1(b)), and upon propagated further through the sample (Fig. 1(c)), its value is sharply then further decreased until reaching its final state. From the 3D reconstructed image results, initiated crack lines were identified exerting a tilted fractured surface at 40-50º to the tensile axis. As shown by results, the presented *in-situ* XCT setup owns remarkable beneficial features.

IV. Conclusions

A new *in-situ* XCT setup has successfully detected evolution of crack initiation and propagation. The devised system offered superior resolution for testing at high temperatures in order to observe the challenging fracturing mechanisms of polycrystalline nickel-based superalloys. The authors believe this setup is further extendable to other systems, including for renewable energy industry.

V. References

[1] le Graverend, J. B., Adrien, J., Cormier, J., Mat Sci & Eng A 695, pp.367-378, 2017.
[2] Schneider, C. A., Rasband, W. S., Eliceiri, K. W., Nature Methods 9, pp.671-675, 2012

Artificial photosynthesis system by using alternate stacked semiconductor nanosheets.

F. Kishimoto*, S. Tsubaki, M. M. Maitani and Y. Wada*

* Department of chemical science and engineering, Graduate school of materials and chemical technology, Tokyo Institute of Technology

e-mail: kishimoto.f.aa@m.titech.ac.jp, yuji-w@apc.titech.ac.jp

Keywords: Photocatalyst, Nanosheets, Layered structure, Visible light induced electron transfer

I. INTRODUCTION

Solar energy conversion systems are promising devices for reducing our dependence on fossil fuels. In particular, artificial photosynthesis systems for a hydrogen production are widely researched. The targeted solar-to-hydrogen conversion efficiency for such an artificial photosynthesis system is 10 %. However at the present moment, the conversion efficiency was reached to 1.1 % at highest[1]. Therefore, new concepts to drastically increase the efficiency are much needed.

In the general artificial photosynthesis systems, the powder of two types of semiconductors are dispersed in a medium, and the electron transfer reaction between the oxygen evolution photocatalysts to the hydrogen evolution photocatalysts is mediated by the dissolved redox couples (Fig. 1(a)). In such a conventional system, the backward electron transfer reaction from the hydrogen evolution photocatalyst to the oxygen evolution photocatalyst is also mediated by the dissolved redox couples. The efficiency of these systems is a consequence of the balance of forward and backward electron transfer reactions. Therefore, the suppression of backward electron transfer reaction to make the electron transfer reaction system 'vectorial' is the most important issue.

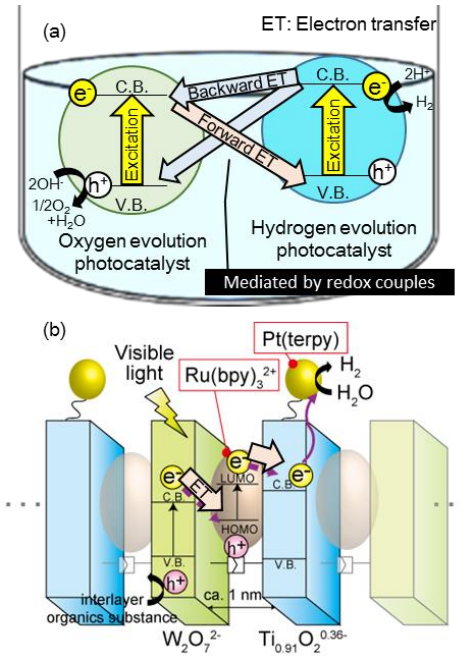

Fig. 1 (a) Conventional artificial photosynthesis system, and (b) proposed artificial photosynthesis by using stacked nanosheets.

In the current study, we proposed that a dye-intercalated alternate-stacked structure (Figure 1(c)), made from thiol-functionalized titanate nanosheets ($Ti_{0.91}O_2^{0.36-}$) and alkene-functionalized tungstate nanosheets ($W_2O_7^{2-}$) via a thiol-ene click reaction[2,3], provides a precisely controlled construction that allows one to understand and control the overall forward and backward electron transfer reactions.

II. RESULTS AND DISCUSSION

We demonstrated the visible-light-induced Z-scheme vectorial electron transfer reactions from the tungstate nanosheets to the titanate nanosheets in the alternate-stacked nanostructure via intercalated $Ru(bpy)_3^{2+}$. The electron injection from the lowest unoccupied molecular orbital (LUMO) level of photoexcited $Ru(bpy)_3^{2+}$ to the titanate conduction band should be as competitive as that to the tungstate conduction band. The rate constants of these processes were determined from the fluorescence decay of $Ru(bpy)_3^{2+}$. The electron transfer reaction from the conduction band of the tungstate to the vacant HOMO level of the photoexcited $Ru(bpy)_3^{2+}$ was demonstrated by a quantitative estimation of electrons stored in the conduction band of the tungstate by means of near-infrared spectroscopy. The electrons reaching the conduction band of the titanate can be transferred to the Pt(terpy) immobilized at the edge of the titanate nanosheets, leading to a hydrogen generation reaction by the reduction of water. We quantitatively determined the amount of hydrogen gas generated and confirmed the photoinduced hydrogen evolution reaction via the Z-scheme vectorial electron transfer reactions in the alternate-stacked nanostructure (Fig. 2).

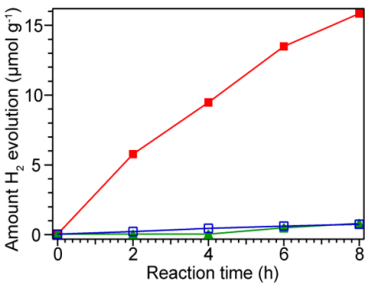

Fig. 2 The amount of hydrogen evolution by using the alternate stacked nanosheets (red), Pt(terpy) modified layered titanate (blue), and layered titanate (green).

REFERENCES

[1] Q. Wang, *et al*, *Nat. Mater.*, *15*, 611, 2016.
[2] F. Kishimoto, *et al*, *RSC Adv.*, *6*, 73830, 2016.
[3] F. Kishimoto, *et al*, *Phys. Chem. Chem. Phys.*, *16*, 872, 2014.

NO Emission from a single coal particle combustion in O_2/N_2 and O_2/CO_2 atmospheres

L.W. Wang*, N. Karimi and M.C. Paul
*School of Engineering, University of Glasgow, United Kingdom
e-mail: l.wang.4@research.gla.ac.uk

Keywords: single coal particle, NO, O_2/CO_2 atmospheres

I. INTRODUCTION

NOx emissions generated during pulverized coal combustion are environmentally harmful, and may lead to corrosion of combustion equipment, photochemical smog and acid rain [1]. Oxy-fuel combustion is regarded as one promising technology to reduce and control pollutant emissions. Oxy-fuel combustion technology is still to be developed, therefore, NOx emissions from coal combustion under O_2/CO_2 atmospheres need to be investigated. In this study, NO were focused.

II. NUMEICAL MODEL

Modelling of NOx emissions during a single coal combustion was from the existing experimental investigation work [2]. Single coal particles were injected into a drop-tube furnace, and were ignited and burned in both quiescent O_2/N_2 and O_2/CO_2 atmospheres with oxygen concentration varying from 40% to 100%. The coal particles consisted of 13.2% moisture, 48.6% volatile matter, 29.8% fixed carbon and 8.4% ash based on proximate analysis [2], in which the contents of C, H, O, N and S were 66.2%, 4.0%, 18.6%, 0.9% and 0.7% respectively.

The numerical simulations were conducted using an Euler-Lagrange model. The weighted-sum-of-gray-gases model (WSGGM), P-1 radiation model (spherical harmonic method), single kinetic rate devolatilization model and multiple-surface-reactions combustion model (e.g., char-O_2, char-CO_2, and char-H_2O) were used for the modelling. The flow field was solved using the standard k-ε turbulence model with the SIMPLE algorithm for velocity-pressure coupling. Gravity was enabled as well when running these numerical simulations. The simulations were run in ANSYS FLUENT. The operating conditions refered to the conducted experiments in ref. [2].

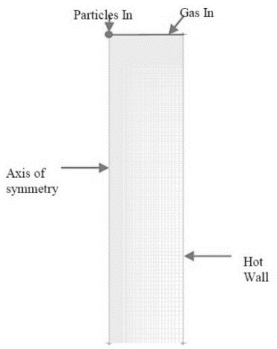

Figure 1. 2D axisymmetric geometry with mesh

III. RESULTS

1. Validation of Numerical Model

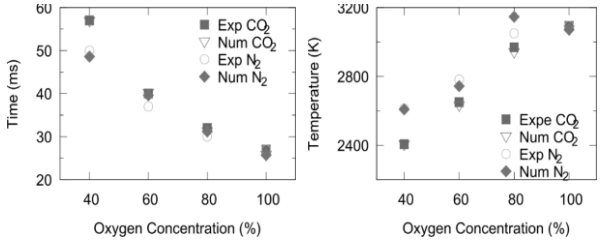

Figure 1. Compared particle life time and temperature of numerical and experimental data

The numerical model was valid as the numerical results matched well with experimental data.

2. NO Emission

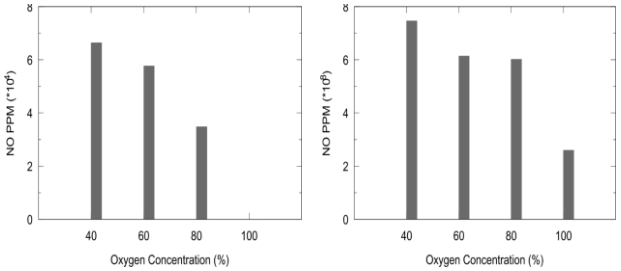

Figure 3. NO ppm during single coal particle combustion

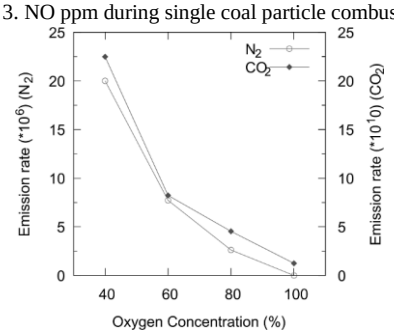

It's clearly shown that, the NO concentration decreased while oxygen concentration increasing in both O_2/N_2 and O_2/CO_2 atmospheres, and it was much lower when coal particle was burned under O_2/CO_2 gas conditions than O_2/N_2 gas conditions. This is also proved by the results of NO emission generation rate.

REFERENCES

[1] P. Glarborg, A.D Jensen, J.E Johnsson, *Progress in Energy and Ccombustion Science*, p, 89, 29(2), 2003.

[2] T. Maffei, R. Khatami, S. Pierucci, E. Ranzi, Y.A. Levendis, *Combustion and Flame*, p. 2559, 160, 2013.

CO_2 transport across microalgae Euglena gracilis lipid membrane: A molecular dynamics study

R. Manrique[1], A. Culaba[1], I. Watson[2]

Mechanical Engineering, De La Salle University Philippines

Systems Power and Energy, University of Glasgow, Scotland UK
e-mail: robby_manrique@dlsu.edu.ph

Keywords: Microalgae, CO_2, biofixation, molecular dynamics

I. INTRODUCTION

Annual global CO_2 emissions of the combined coal fired power plant in the world emits roughly 2 billion tons which was forecasted to increase in the next decades as developing countries had invested mostly on cheap energy such as coal. With the threat of global warming due to the increasing concentration of anthropogenic CO_2, several methods and technology for carbon capture had pushed numerous researchers to design and develop materials. One of the emerging methods for CO_2 capture which was believed to be the most important and most effective way of directly converting CO_2 into biomass is thru the biological approach. Photosynthetic microorganisms such as microalgae utilizes CO_2 to produce biomass, wherein, this biomass can be processed into a variety of bioproducts such as biofuels and other high value compounds suitable for aquaculture, pharmaceuticals, and nutraceuticals to name a few. While terrestrial plants are expected to contribute 3 – 6% reduction on CO_2 emissions globally, microalgae are forecasted to perform better mainly due to their better conversion efficiency of about 10 – 50% [1]. Reports have shown that 1kg of microalgae can sequester 1.3 – 1.88 kg of CO_2 [2]. To fully maximize the biofixation capability of microalgae, an effective absorption process should be realized by elucidating the connections of crucial operating cultivation conditions such as temperature and salinity. The current study will conduct an atomic scale study on the effect of temperature and salinity on the transport of CO_2 across the microalgae lipid membrane using molecular dynamics (MD) simulation.

A. Microalgae lipid membrane

The lipid membrane plays a very important role in every living organisms as it controls and regulates the transport of small molecules (O_2, H_2O, CO_2 etc) into the intra cellular part of the cell for their metabolic needs. The lipid membrane is basically composed of phospholipids arranged parallel with each other and protects the internal organelles of the microalgae cell from the environment. The phospholipids used for this study are dipalmitoyl: (1) phosphatidylglycerol (DPPG), phosphatidylcholine (DPPC) and phosphatidylethanolamine (DPPE) which are all present in microalgae *Euglena gracilis* specie [3].

B. Molecular Dynamics

MD has been the leading theoretical tools for the study of biological molecules particularly lipids, nucleic acids, proteins and carbohydrates. MD "brings to life" theoretical models that opens a better understanding on traditional experiments. Figure 1 shows the model for the microalgae lipid membrane composed of a mixture of DPPG, DPPC and DPPE phospholipids solvated with water molecules. Three lipid membrane structures at different salinities (50, 200 and 300 mM) was created and equilibrated at 300K and 1 bar prior to permeation calculations.

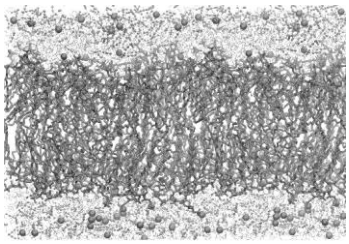

Figure 1. Microalgae lipid membrane visualized by VMD [4].

C. CO_2 permeation calculations

In thermodynamics, the one that governs the movement of a molecule is due to its free energy gradient. Hence, calculating the free energies can provide information on the permeation process of any molecule. To describe the effects of salinity and temperature on the CO_2 transport, the permeation coefficient of CO_2 molecule was calculated in each lipid membrane structures using the equation:

$$\Delta G(z) = G(z) - G(z_0) = \mu_{ex}(z) - \mu_{ex}(z_0) \quad (1)$$

In here, $\Delta G(z)$ is the free energy gradient of the CO_2 molecule along the bilayer normal (z-axis) which also represent the change in chemical potential (μ_{ex}) calculated using equation 2. The < … > indicates the interaction of the CO_2 molecule with the rest of the system.

$$\mu_{ex} = -k_B T ln \langle \beta \frac{P_{ext} V}{(N+1)} exp[-\beta \Delta U] \rangle_N \quad (2)$$

REFERENCES

[1] J. Cheng, Y. Huang, J. Feng, J. Sun, J. Zhou, K. Cen. Improving CO2 fixation efficiency by optimizing Chlorella PYZU1 culture conditions in sequential batch reactors. Bioresource of Technology, 144, 321-327.

[2] HT. Hsueh, H. Chu, ST. Yun, A batch study of the biofixation of carbon dioxide in the absorbed solution from from a chemical wet scrubber by hot spring and marine algae, Chemosphere, 2007.

[3] A. Regnault, D. Chervin, A, Chammai, F. Piton, R. Calvayrac, P. Mazliak, Lipid composition of Euglena gracilis in relation to carbon-nitrogen balance, Phytochemistry, p.725, 1995.

[4] W. Humprey, A Dalke, K. Schulten, VMD: Visual Molecular Dynamics, Journal of Molecular Graphics, p 33, 1996.

Deformation of Space Membrane Structures with Curved Thin-film Solar Cell

M. Matsushita*, O. Mori**, N. Okuizumi**, Y. Satou**, T. Iwasa*** and S. Matunaga****
*Department of Mechanical and Aerospace Engineering, Tokyo Institute of Technology, Japan
**Institute of Space and Astronautical Science, Japan Aerospace Exploration Agency, Japan
***Department of Mechanical and Aerospace Engineering, Tottori University, Japan
****Department of Mechanical Engineering, School of Engineering, Tokyo Institute of Technology, Japan
e-mail: matsushita@lss.mes.titech.ac.jp

Keywords: Spacecraft, Membrane Structures, Solar Sail, Solar Cell, Wrinkle

I. INTRODUCTION

In an actual operation of a solar power sail, which has a membrane with thin-film solar cells, IKAROS, distortion of a sail reflecting photon flux causes in-plane torque. The torque should be predicted because the propellant was wasted to control the spin rate. The deformation is considered to be induced by curved thin-film solar cells [1]. It is important to build a model of a membrane with curved cells and evaluate the shape for membrane structures, such as solar power sails and space solar power systems. In this paper, as a preliminary study, a part of a spinning solar sail is simply modeled as a membrane with a curved cell (Fig. 1) in an explicit dynamic, nonlinear finite element simulation to investigate local wrinkles near the curved cell under varying uniaxial tension. The model is verified using measured shapes in experiments.

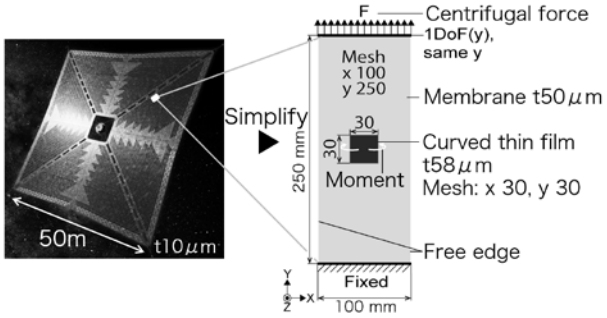

Figure 1. A JAXA's next spinning solar power sail and a finite element model of a simplified model of a part of the sail

II. FINITE ELEMENT MODEL

A finite element model is shown in Fig. 1. Uniaxial tension force is adopted because radial force is more dominant than circumferential force in the spinning solar sail. The rectangle membrane is adopted because it is assumed that wrinkle occurs near the cell along tension. A PET membrane and an amorphous silicon thin-film solar cell were used in the simulations and experiments. Tension is changed to 9800, 980, 98 and 9.8 mN with reference to the IKAROS.

III. EXPERIMENTAL METHOD

Figure 2 shows a schematic diagram of an experimental setup. The membrane was pulled by weights and fixed on a tension test apparatus. The shapes under each tension were measured using a 3D scanner.

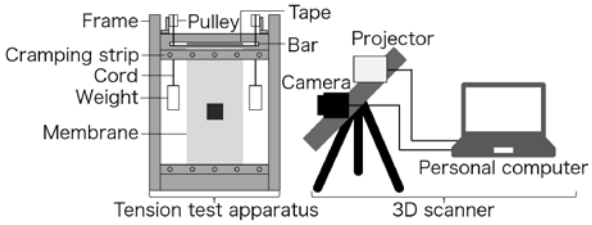

Figure 2. A schematic diagram of an experimental setup

IV. RESULTS AND DISCUSSIONS

The numerical shapes qualitatively match the measured shapes under each tension force. Wrinkle lines near both lateral sides of the curved cell are bent by curvature of the cell and become the X-shape, which occurs even if tension is changed. In one example, figure 3 shows contour plots of out-of-plane position of the membrane under 98 mN in the simulation and experiment.

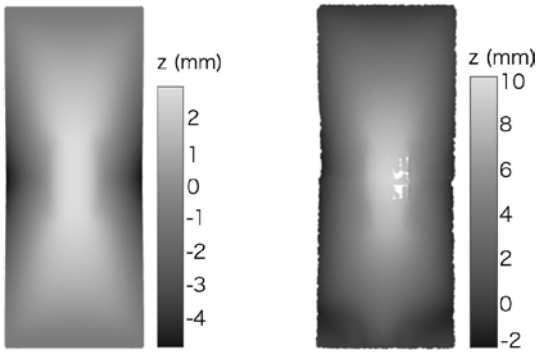

(a) Simulation. (b) Experiment.

Figure 3. Shapes of a membrane with a curved thin-film solar cell under 98 mN tension. Holes in (b) are lack of data

V. CONCLUTION

We measured and simulated wrinkles in the membrane with the curved cell under tension as a simplified model of a part of the solar sail. The finite element model was qualitatively verified by the experiments. The X-shaped wrinkles occurred due to tension and the curved cell.

REFERENCES

[1] Y. Satou, O. Mori, N. Okuizumi, Y. Shirasawa, H. Furuya and H. Sakamoto, *Proceedings of SciTech2015*, p.1-11, Jan 2015.

Numerical Equilibrium Model of Food Waste Gasification

A.Nadirah Izaharuddin* and Manosh Paul*
*Systems, Power & Energy Research Division, School of Engineering, University of Glasgow, Glasgow G12 8QQ, United Kingdom
e-mail: a.binti-izaharuddin.1@research.gla.ac.uk

Keywords: Municipal solid waste (MSW); Food waste; Gasification; Equilibrium model

I. INTRODUCTION

Municipal solid waste (MSW) is one of the potential feedstocks that could be processed through gasification to generate gaseous fuel products known as synthesis gas (syngas). The gasification technology is important in the current context, and waste-to-energy plants are having high-efficiency power production in utilizing MSW as fuel rather than other sources of energy [1].

Food waste refers to appropriate food for human that discarded whether it is kept after expiry date or not. Usually, these food have been thrown away because of spoiling and other reasons such as oversupply due to markets or the consumer shopping habits. The Waste & Resources Action Programme (WRAP) and Department for Environment Food & Rural Affairs (DEFRA) reported abount 15 million tonnes of food and drink were wasted in the food chain in 2013 which is equivalent to around one third of the 41 million tonnes of food that is bought annually in the UK [2, 3]

II. METHODOLODY

Food waste samples were collected in Glasgow, which include of East, West and South area, such as at Universities, college, household, and restaurants. An equilibrium model of gasification process has been developed through MatLab code, at 0-40% moisture content, 1023K - 1173K gasification temperature, and 0.2-0.4 equivalence ratio. Through this model, the ultimate analysis of food waste has been analysed in global gasification process.

Furthermore, the optimum conditions of food waste gasification has been analysed by statistical method, to find the optimum conditions of parameters, producer gas, calorific value and exergy analysis.

III. RESULT & DISCUSSION

To find the optimum conditions of gasification process, a sensitivity analysis is carried out in the stated moisture content range, gasification temperature range and equivalence ratio range. Figure 1 shows the moisture content analysis with gasification temperature at 1123 K at 0.28 equivalence ratio. Based on the figure, hydrogen (H_2), carbon dioxide (CO_2), and methane (CH_4) increased with increasing moisture content, refer to water gas reaction, shift reaction and methanation reaction, while carbon monoxide (CO), nitrogen (N_2) and CV decreased.

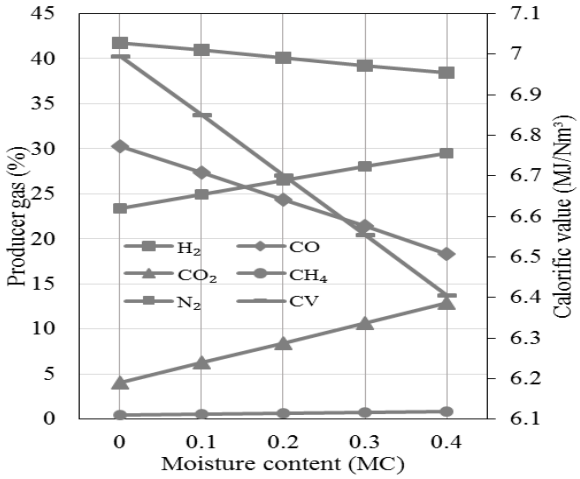

Figure 1 Moisture content analysis with gasification temperature at 1123K at 0.28 equivalence ratio

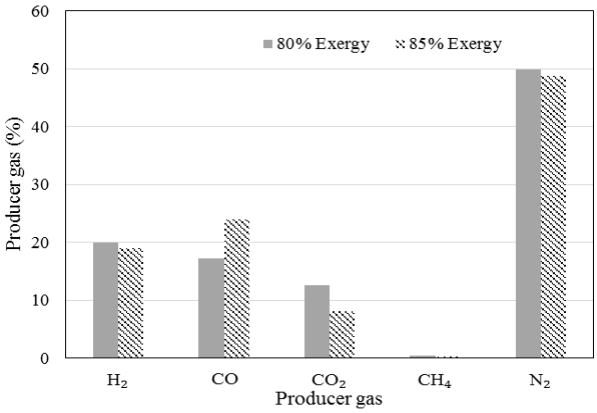

Figure 2 Producer gas with exergy limitation

Figure 2 shows the optimum conditions of producer gas with 80% exergy and 85% exergy limitation, which carbon dioxide has low result in high exergy.

IV. REFERENCES

1. Speight, R.L.a.J.G., *Gasification for Synthetic Fuel Production* Fundamentals, Processes, and Applications 2015: Woodhead Publishing
2. WRAP, *Estimates of Food and Packaging Waste in the UK Grocery Retail and Hospitality Supply Chains*. 2015.
3. Affairs, D.f.E.F.a.R., *Digest of waste and resource statistics-2016 Edition*, E.F.R. Affairs, Editor. 2016.

Molecular basis for Hsp104-mediated prion propagation in yeast

Y. Nakagawa*, M. Tanaka** and H. Taguchi*
* Institute of Innovative Research, Tokyo Institute of Technology, Japan
**RIKEN Brain Science Institute, Japan
e-mail: nakagawa.y.au@m.titech.ac.jp

Keywords: Amyloid fiber, Chaperone, Aggregation

I. INTRODUCTION

Several neurodegenerative diseases, including Alzheimer's disease, Huntington's disease, and prion disease, are caused by misfolding and subsequent aggregation of proteins. Recent studies revealed that such protein aggregates as well as prion aggregates show cell-to-cell transmission, suggesting that propagation of protein aggregates are not specific to prion protein but rather are universal [1]. In the yeast prion system, the molecular chaperone Hsp104, a hexametric AAA+ ATPase, in concert with Ssa1 (a member of the Hsp70 family) and Sis1 (a member of the Hsp40 family), is suggested to play crucial roles in the apparently conflicting two steps of prion propagation: the acceleration of amyloid formation and the disaggregation of amyloid [2]. Yet, the molecular basis of Hsp104-mediated prion propagation is poorly understood. Here, we attempted to reveal how the Hsp104/Ssa1/Sis1 chaperone machinery accelerates Sup35NM, a fragment of yeast prion protein Sup35, and disaggregates Sup35NM amyloid *in vitro*. In the UKJEEL poster session, I will further discuss material development using the polymorphic structure of amyloid fibers to develop energy systems.

II. METHODS

We first established the purification protocol for the three chaperones and successfully confirmed the hexamerization of Hsp104. Using the chaperone system, we performed the disaggregation assay and the fiber acceleration assay.

A. Disaggregation assay

Sup35NM amyloid fibrils were incubated in the presence of chaperones (Hsp104, Ssa1, Sis1) with ATP and an ATP regeneration system at 30°C. The mixtures of Sup35NM fibrils-chaperones were centrifuged at 200,000× g for 30 min. We quantified Sup35NM levels in the supernatant or pellet by western blotting with anti-NM rabbit monoclonal antibodies.

B. Fiber acceleration assay

The fiber acceleration of the Sup35NM monomer was performed in the presence of chaperones (Hsp104, Ssa1, Sis1) with ATP and an ATP regeneration system. The extent of fiber formation were measured by Thioflavin T binding to Sup35NM fibers. The length of amyloid fibers was observed by Atomic Force Microscopy (AFM).

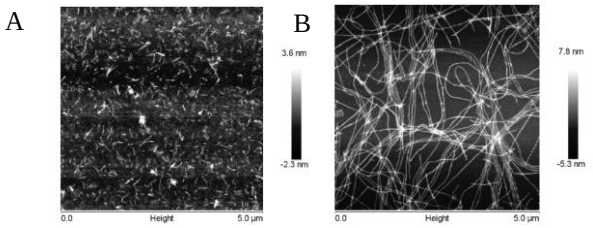

Figure 1. AFM image of amyloid fibers with chaperones (Hsp104, Ssa1, and Sis1) (A), without chaperones (B)

III. RESULTS

A. Disaggregation of the Sup35NM amyloid

We found that the disaggregation of Sup35NM amyloid was promoted by the Hsp104/Ssa1/Sis1 complex in an ATP-dependent manner.

B. Acceleration of amyloid formation

The amyloid formation of Sup35NM was significantly accelerated by the Hsp104/Ssa1/Sis1 complex in an ATP-dependent manner. In addition, the acceleration of fiber formation was the temperature dependent.

The length of amyloid fibers formed in the presence of Hsp104/Ssa1/Sis1 was shorter than the length of amyloid fibers formed without chaperones (Fig.1). In addition, the length of the fiber formed by chaperones became shorter with increasing temperature.

IV. DISCUSSION & CONCLUSIONS

The Hsp104, Ssa1, and Sis1 chaperones were all required to disaggregate the Sup35NM amyloid and accelerate Sup35NM fiber formation. The AFM results indicated that both the seeding reaction and fiber fragmentation were involved in accelerating Sup35NM fiber formation. The distinct disaggregation efficiency is suggested to impact amyloid fiber length.

REFERENCES

[1] J. Guo, S. Narasimhan, L. Changolkar, Z. He, A. Stieber, B. Zhang, RJ. Gathagan, M. Iba, J. McBride, J. Trojanowski, V. Lee (2016) *J Exp Med*. 14;213(12):2635-2654

[2] J. Winkler, J. Tyedmers, B. Bukau (2012) *Journal of Structural Biology*, 179, 152-160

Understanding the regulatory mechanism of triacylglycerol biosynthesis to improve oil productivity in the green microalgae

Nur Akmalia Hidayati*, Yui-Yamada Oshima*, Masako Iwai*, [1], Koichi Hori*, [1], Takeshi Obayashi[2], Hideya Fukuzawa[3], Mie Shimojima*, Hiroyuki Ohta*, [1]

*Department of Biological Sciences, Tokyo Institute of Technology, Japan, [1]CREST, JST, [2]Tohoku University, Japan, [3]Kyoto University, Japan
e-mail: hidayati.n.aa@m.titech.ac.jp

Keywords: triacylglycerol, transcription factor, nutrient starvation, *Chlamydomonas reinhardtii*

I. INTRODUCTION

Increased energy demand in the public and private sector, which includes transportation, industries, and home appliances address the issues on energy security since the fossil fuel has become depleted nowadays [1]. Shifting from the traditional energy supply to renewables to achieve a sustainable energy system has widely become one of the major concerns by the global researchers. The solution includes utilization of microalgae as the renewable feedstock to produce biofuel [2]. The application of microalgae features some promising potential than the traditional biofuel land crops; it can be cultivated in a non-arable land so that it will not compete with food and agriculture [3]. As autotrophs, microalgae has the ability by converting sunlight to fix atmospheric CO_2 into biomass, thus mitigating the carbon pollutants through its process [4]. It provides higher biomass productivity and contained higher oil's percentage than plants [5, 6]. More importantly, neutral lipid in the form of triacylglycerol (TAG) from microalgae can serve as primary feedstock for fuel production via transesterification [5, 7].

TAG is mainly observed as primary lipid storage under nutrient- starved condition such as Nitrogen (N), Sulfur (S), Zinc (Zn) and Phosphorus (P) in *C.reinhardtii* [8]. Increased oil content up to 80% dry weight was reached by some microalgae by shifting their metabolic system into oil-producing mode induced by nutrient starvation [5, 6]. Rapid increase in TAG accumulation under nutrient-starved condition, such as N-starvation brought the drawback in overall biomass yield due to inhibition of cell division and decreased photosynthetic activity. Meanwhile, the inhibition of photosynthetic activity under P-starvation is not as severe as N-starvation; therefore the growth is relatively compromised.

The basic knowledge of P-starvation is taken into consideration to reveal regulatory mechanism of lipid accumulation to enhance oil productivity, through identification of novel transcription factor (TF) based on co-expression analysis. Furthermore, this novel transcription factor is predicted to be involved in TAG accumulation and other metabolic process under P-starved condition in *C.reinhardtii.*

II. RESULT

A. Co-expression analysis showed highly inducible transcription factor under P-starvation that co-expressed with DGAT2 gene

A transcription factor (TF) that has similar expression pattern with diacylglycerol acyltransferase 2 (*DGAT2)* gene (the gene that involved in the last step of TAG synthesis) was identified. This TF possesses a similarity with *Arabidopsis thaliana MYB64* gene and clarified as its homolog. Under P-starvation, a significant increased up to 12-fold was reached, indicating this novel TF might serve as a regulator of P-starvation in *C. reinhardtii.*

B. Expression level of DGAT2 gene correlated with TAG accumulation under P-starvation

By analyzing mutant line of this inducible TF, a decreased in TAG accumulation is occurred after 8-day cultivation under P-starved condition. Down-regulation of *DGAT2* gene is obviously observed from the transcriptomics analysis of the mutant under P-deficient condition at 4-day culture. Therefore, an increased level of TAG in overexpression lines might be due to correlation of this TF with several genes involved in carbon metabolism, specifically later step of TAG synthesis.

REFERENCES

[1] Tan, K.W.M., Lee, Y. K., *Biotechnol Biofuels*., 9, 255-268, 2016.

[2] Goncalves, E.C., Koh, J., Zhu, N., Yoo, M., Chen, S., Matsuo. T., Johnson, J.V., Rathinasabapathi, B., *Plant J.*, 85, 743-757, 2016.

[3] Moody, J.W., McGinty, C.M., Quinn, J.C., *Proc. Natl. Acad. Sci.*, 111, 8691-8696, 2014.

[4] Guiheneuf, F., Khan, A., Tran, L.P., *Front. Plant Sci.*, 7, 400-407, 2016.

[5] Chisti, Y., *Biotechnol. Adv.*, 25, 294-306, 2006.

[6]Spolaore, P., Joannis-Cassan, C., Duran, E., Isambert, A. N., *J. Biosci. Bioeng.*, 101, 87-96, 2006.

[7]Foley, P. M., Beach, E.S., Zimmerman, J.B., *Green Chem.*, 13, 1399-1405, 2011.

[8]Iwai, M., Ikeda, K., Shimojima, M., Ohta, H., *Plant Biotech. J.*, 12, 808-819, 2014.

Linearizing energy supply technology characteristic curves: a comparison of methods

B. Pickering* and R. Choudhary*
*Department of Engineering, University of Cambridge, United Kingdom
e-mail: bp325@cam.ac.uk

Keywords: Energy system optimization, Mixed integer linear programming, Piecewise linearization, District energy

Increasingly, computational methods are being designed to model complex energy systems. In doing so, the realistic operation of supply technologies cannot be fully represented without loss of model tractability. Technologies are usually described as having a nominal efficiency to linearize their operation for use in linear (LP) or mixed integer linear (MILP) programming. But, the part load efficiency of many energy supply technologies is inherently nonlinear. Representative curves available from The Society of Heating, Air-conditioning and Sanitary Engineers of Japan (SHASE) [1] show that these nonlinearities are particularly evident in cooling technologies and combined heat and power plantss.

Using a nominal efficiency, it is possible to avoid binary and integer decision variables in optimization, leading to an LP model which can solve quickly. The introduction of one binary variable per technology-location increases solution time, but allows the nonlinear curve to be represented by several 'y = mx + C' lines, which effectively segment the nonlinear curve into straight lines (figure 1).

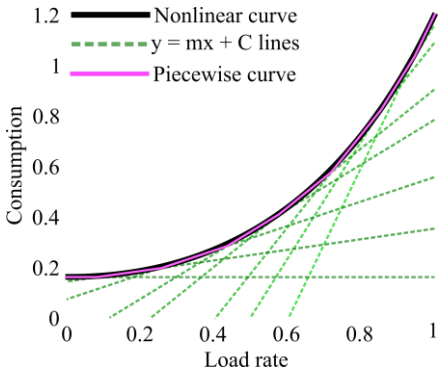

Figure 1: Representing a nonlinear constraint with several 'y=mx+C' constraints, describing a piecewise curve.

When applied to the same optimal energy dispatch problem, [3] showed that linearizing part-load curves allows technologies to be represented in MILP models, improving solution time compared to a metaheuristic model optimizing the same problem. However, a time penalty of up to two orders of magnitude was still present when using piecewise curves instead of nominal efficiency. In [2], improvements were made by considering the optimal number of breakpoints along the piecewise curve and the use of bounding constraints (as shown in figure 1) to describe the curve, rather than the conventional Special Ordered Sets of order 2 (SOS2). Again, solution time was improved, but larger spatial scales and longer temporal scales were still out of reach.

As few as two of these lines allow the curve to be sufficiently represented [2]. However, it may be possible to further simplify the problem without loss of accuracy, by considering only one 'y = mx + C' line to describe the nonlinear curve. Although feasible low-load operation cases may exist, setting a minimum capacity below which a technology cannot run allows a single line to better describe the remaining part-load curve. Figure 2 shows these varying linearization methods applied to the part-load curve of an electric chiller.

Each method is applied to technologies which are optimized to meet the demand of a representative district, with electrical, cooling, and heating demands. Solution times, objective function values, and optimal operation schedules are compared to better understand the effect of model component accuracy. A model designer has the choice to improve accuracy at the cost of increased solution time. This study provides a reference for choosing a trade-off suitable for the energy system problem with which they are faced.

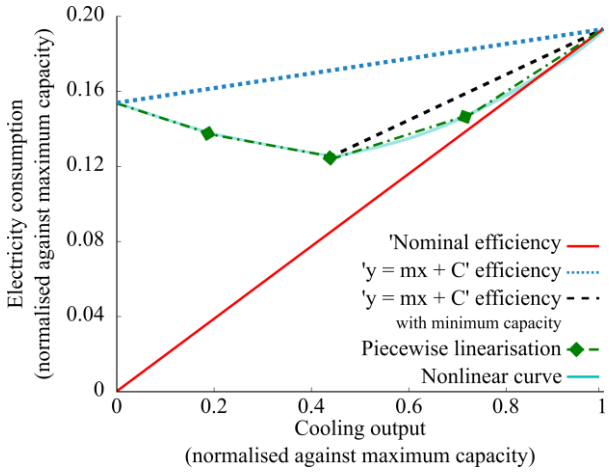

Figure 2: comparison of methods to describe the nonlinear part-load consumption curve of a representative electric chiller.

References

[1] The Society Heating, Air-Conditioning and Sanitary Engineers of Japan (SHASE), S.E. of 2003. *Computer Aided Simulation for Cogeneration Assessment & Design III*. Maruzen publishing.

[2] Pickering, B. and Choudhary, R. 2017. Applying Piecewise Linear Characteristic Curves in District Energy Optimisation. (San Diego, USA, 2017).

[3] Pickering, B., Ikeda, S., Choudhary, R. and Ooka, R. 2016. Comparison of Metaheuristic and Linear Programming Models for the Purpose of Optimising Building Energy Supply Operation Schedule. *12th REHVA World Congress* (Aalborg, Denmark, 2016).

Improving Downdraft Gasifier Stability by Robust Instrumentation and Control Systems

Prashant Kamble, Zakir Khan, Ian Watson*
Systems, Power and Energy Research Division, School of Engineering,
College of Science and Engineering, University of Glasgow, Glasgow, G12 8QQ, UK
*ian.watson@glasgow.ac.uk

Keywords: Gasification; Arduino; Diagnostic and Control, Sensor.

I. INTRODUCTION

The principal objective of this research is to develop a set of robust and inexpensive instrumentation systems to measure gasification parameters and inform control systems to improve gasification performance e.g. temperature, liquid flow and biomass weight for real time mass balance calculations. In the present case nine K-type thermocouples were connected to different positions on an in-house downdraft gasifier that allowed temperature and mass balance profiling. The moisture / bio-oil flow was measured by a liquid flow sensor that gave real time flow rates (L/min) and total quantities (mL) [1]. The Arduino platform was used as the core of the instrumentation and control system and integrated with Makerplot software (GUI). These systems offered a high level of control and robustness for low cost with an open source protocol, allowing other developers to benefit and expand the core of this research. The results from preliminary runs are presented which is currently allowing ignition optimization and overall system improvements..

II. CONTROL STRATEGY

The Arduino Mega ADK microcontroller ATmega2560 board has 16 analog and 54 digital inputs (I/O). The microcontroller interfaces with an Android based mobile on the MAX3421e IC [4]. The nine K-type thermocouples were connected to different positions of the gasifier system and interface with Max 31855 breakout board amplifiers. The amplifier works with any K-type thermocouple with ±2°C to ±6°C accuracy with an output in 0.25ºC increments. The hall liquid flow sensor was connected before the moisture / bio oil collection system. The liquid flow sensor works between -25°C to +80°C with an accuracy ± 10% [2]. The pulse signal is a simple square wave which is converted into L/min. Figure 1 shows the location of the thermocouples (identified as T1 through to T9).

III. RESULTS AND DISCUSSION

Figure 2 shows the temperature data and Figure 3 shows the liquid flow from preliminary gasification runs with Miscanthus (Mx2717). The temperatures measured at the drying (T01), pyrolysis (T02), combustion (T03) and reduction zone (T04) are each below 350 °C for the first 12 min of operation. Subsequently, the pyrolysis and combustion zone temperatures rose significantly, up to 682°C from 12 min to 14 min due to injecting air at a flow rate 55 L/min.

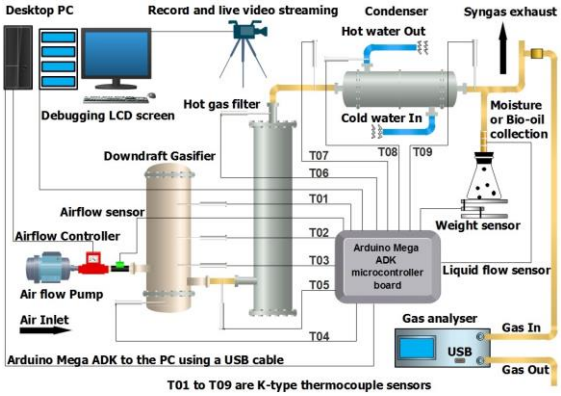

Figure 1. Control strategy of downdraft gasifcation system

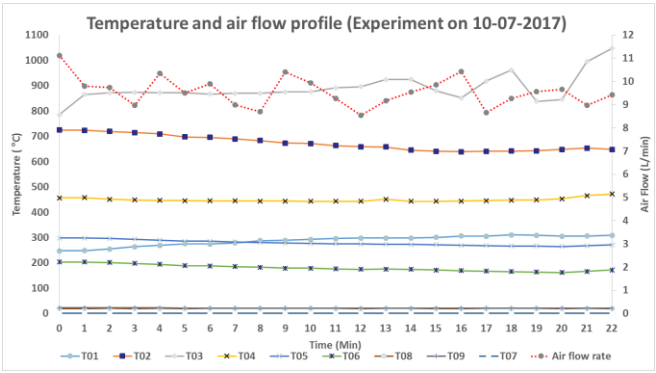

Figure 2. Temperature and air flow profiles

REFERENCES

[1] [2] R.E. Bentley, Long-term drift in mineral-insulated Nicrosil-sheathed type K thermocouples, Sensors and Actuators A: Physical, 24 (1990) 21-26.

[2] M.S. McMunn, A time-sorting pitfall trap and temperature datalogger for the sampling of surface-active arthropods, HardwareX, 1 (2017) 38-45.

Measurement of thermophysical properties and instrumentation for thermo-spectroscopy

M. Ryu* and J. Morikawa*

*Department of Material Science and Engineering, Tokyo institute of technology, Japan
e-mail: ryu.m.ab@m.titech.ac.jp, morikawa.j.aa@m.titech.ac.jp

Keywords: thermophysical property, thermal imaging, infrared spectrum imaging, liquid crystal, phase transition

I. INTRODUCTION

The effect of molecular alignment plays an important role in the thermophysical properties of soft materials. The liquid crystals (LCs) were extensively investigated for the model of the anisotropic thermal properties. The temperature wave analysis method (TWA) has been applied to measure the heat transfer properties of LCs.

TWA method was originally developed for the thermal diffusivity measurement of thin film organic materials from the determination of temperature wave phase delay in the sample layer. The method into simultaneous measurement of thermal diffusivity α, thermal effusivity e, thermal conductivity λ, and heat capacity per unit volume has been more practically improved recently [1].

The azobenzene monolayer attached on the substrate surface induced a reversible change of LC alignment mode, which is known as a command surface. In this study, TWA method was applied to measure the photo induced anchoring transition of azo dendrimer dissolved in a liquid crystal (Fig. 1) [1].

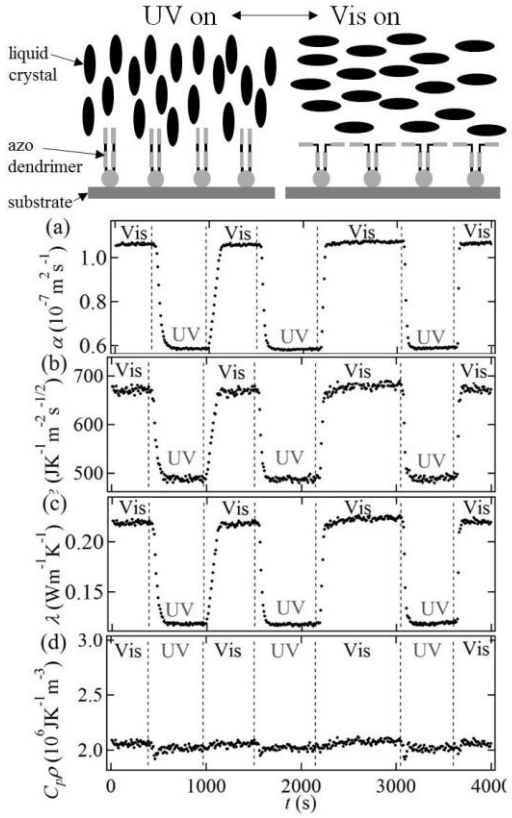

Figure 1. (a) Thermal diffusivity α, (b) thermal effusivity e (c) thermal conductivity λ (d) heat capacity per unit volume as a function of time during the irradiation of light switching between visible (420 nm) and UV (365 nm).

II. RESULTS

For the thermal management of the composite material or the devices, not only single point measurement, but also imaging measurement becomes important. To expand the one-point thermal property measurement into in-plane imaging measurement, a novel system developed that combined two imaging techniques enabled simultaneous measurements of IR spectroscopic and thermal imaging at micro scale [2-3].

The thermal and the spectroscopic images are alternatively recorded with the synchronization signal of a chopper which attains the high simultaneity in the measurement. We report the high possibility of the system to study dynamic phase change at high frequency (200 Hz) and demonstrate that this analytical tool is a new system for the simultaneous thermal and chemical structural analysis of materials at microscale in the dynamic state.

REFERENCES

[1] M. Ryu, H. Takezoe, O. Haba, K. Yonetake, J. Morikawa, *Appl. Phys. Lett.*, p. 107, 2015.

[2] M. Ryu, M. Romano, J.C. Batsale, C. Pradere, J. Morikawa, *Quantitative InfraRed Thermography J.*, 10.21611, 2016

[3] M. Ryu, J.A. Kimber, T. Sato, R. Nakatani, T. Hayakawa, M. Romano, C. Pradere, A.A. Hovhannisyan, S.G. Kazarian, J. Morikawa, , 2017

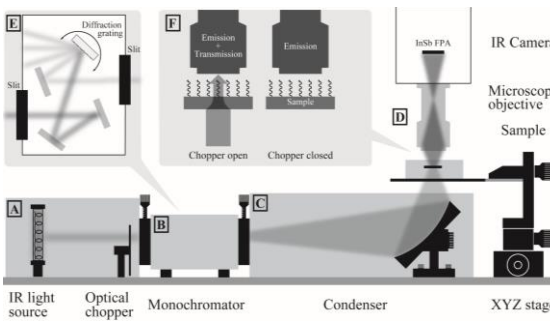

Figure 2. (A) Ceramic heater (light source), (B) grating monochromator to select the IR wavelength (CT-10, JASCO Corporation), (C) condenser module with a parabolic mirror, (D) thin hot stage (S84, ST Japan) acting also as a sample holder place in a XYZ stage and the IR camera (Phoenix, Indigo). (E) Schematic explanation concerning the functioning of the monochromator. (F) Optical signal obtained during open chopper state and closed chopper state: Measuring setup for High frequency dynamic simultaneous microscopic measurements of thermal and spectroscopic image in mid Infrared wavelength.

Modelling of stand-alone solar electrical and solar thermal solutions for remote regions

Stelios Gavrielides, Ian Watson

Systems, Power & Energy Research Division, School of Engineering, University of Glasgow, UK
e-mail: ian.watson@glasgow.ac.uk

Keywords: solar, solar photovoltaic, solar thermal, storage

Introduction A solar PV and a solar thermal model were created as a standalone sustainable energy scheme incorporating a thermal storage tank. The model can estimate the size of the solar farm required to cover the energy needs of any number of houses.

Introduction: Photovoltaic model The photovoltaic effect, is the process of directly converting solar electromagnetic radiation to electricity. The model allowed for observations on the performance behaviour of the PV module when varying solar irradiance and varying the operating cell temperature, showing that both factors influence the performance significantly but solar irradiance is by far the most dominant factor.

The PV model was then connected in series and in parallel to create a PV array configuration, incorporating a MPPT algorithm (P&O). This model was then merged with the model of Wind and Hydro schemes (Shoaib and Watson, UKJEEL 2017) thus creating a comprehensive electrical model. The PV model was also configured to estimate the available electrical energy during a day under the assumption that the solar irradiance follows a sinusoidal distribution. With the assumption that the sun rises at 6:00am, and by incorporating the average UK house electricity demand daily profile, graphical representations such as figure 1 are possible, which is a 3x3 array for G= $650 W/m^2$.

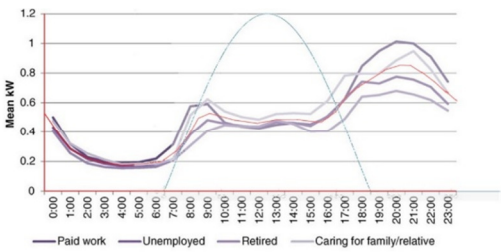

Figure 1 – Combination of daily available electricity and electricity demand for a typical UK house [1]

Solar thermal and thermal energy storage model The importance of thermal energy in the UK cannot be neglected since it accounts for roughly 50% of the total energy needs of the country. The developed model concerns solar flat plate heat collectors and the mathematical model is described by the following equation.

$$Q_u = A_c \times [n_o G - a_1(T_m - T_a) - a_2(T_m - T_a)]$$

The thermal model can produce a graphical representation of the available thermal energy during the day. Combined with the average thermal energy daily profile of a typical UK house, the graphical representation shown in figure 2 is produced.

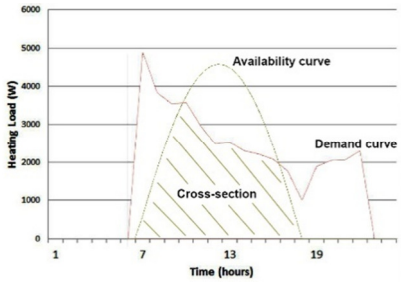

Figure 2 – Combination of the thermal energy availability and requirement along with the area measuring guide. [3]

The integrated model The three scenarios examined are shown in Table 1. The integrated model is created in excel and takes as input the area measurements from the graphs produced by the models (figs 1,2). It calculates the available energy, the demand, the amount of energy that could be directly provided, the maximum energy that could be stored and the energy that should be stored to cover the user's needs and the required tank capacities to do so. It incorporates estimations on the heat losses for the thermal energy storage tank in stand-by conditions in 12, 24 and 48 hrs. All estimations are made for one typical UK house and can be scaled to any number of houses.

Table 1 – Scenarios used in Integrated model

Solar Photovoltaic model				
Scenario 1	3x3 Array	$420 W/m^2$	$650 W/m^2$	$1000 W/m^2$
Scenario 2	4x4 Array	$420 W/m^2$	$650 W/m^2$	$1000 W/m^2$
Scenario 3	4x3 Array	$420 W/m^2$	$650 W/m^2$	$1000 W/m^2$
Solar Thermal model				
Scenario 1	6 collectors	$420 W/m^2$	$650 W/m^2$	$1000 W/m^2$
Scenario 2	10 collectors	$420 W/m^2$	$650 W/m^2$	$1000 W/m^2$
Scenario 3	8 collectors	$420 W/m^2$	$650 W/m^2$	$1000 W/m^2$

References. [1]Svehla, K.M., 2011. A Specification for Measuring Domestic Energy Demand Profiles. [2] Svehla, K.M., 2011. A Specification for Measuring Domestic Energy Demand Profiles.
[3] Nick Kelly, Paul Tuohy (2012) Future Energy Demand in the Domestic Sector, Department of Mechanical and Aerospace Engineering, University of Strathclyde, Glasgow.: Research Unit (ESRU).

Thermal and Electrical Properties of Methylammonium Lead Iodide Perovskite Compact Before and After Phase Transition

Seiya Sugawara*, Tamotsu Sato*, Toshihiro Isobe*, Akira Nakajima*, Sachiko Matsushita*
*Department of Materials Science and Engineering, Tokyo Institute of Technology, Japan
e-mail: sugawara.s.ab@m.titech.ac.jp

Keywords: Thermoelectric, Perovskite, Thermal conductivity, Electric resistivity, Thermal expansion

I. INTRODUCTION

Due to the demand for renewable energy, thermo-electric materials that can convert heat energy to electric energy have attracted wide attention because of their unique ability to convert wasted heat into an energy resource [1]. In such thermoelectric materials, charged carriers diffuse from the hot end to the cold end, generating an electric potential under a given temperature gradient across the material. The thermoelectric figure of merit, zT, is often used as an indicator of the maximum efficiency of a thermoelectric material and a lower ρ and lower κ are required to improve the thermoelectric efficiency (ρ is the electrical resistivity and κ is the thermal conductivity).

Most of thermoelectric materials have exhibited high thermoelectric efficiency at temperatures of over several hundred Kelvin, but only a limited number of materials can work efficiently in the temperature region between room temperature (RT) and 130 °C. He, et al. computationally demonstrated that methylammonium lead halide perovskite ($CH_3NH_3PbI_3$), which recognized as a cost-effective and high-conversion-efficiency photovoltaic material, may be a promising material in this RT region [2]. Even though some studies revealed the electrical properties and thermal properties of $CH_3NH_3PbI_3$ for temperatures below RT, there is no report on the thermoelectric properties in the range of 30-130 °C. In this paper, we firstly report these properties, ρ and κ, in this RT region and also report the easy fabrication method of $CH_3NH_3PbI_3$ compacts, that enable us to measure these characteristics.

II. METHODS

CH_3NH_3I and PbI_2 powders were weighed to the target composition 1:1 (mol/mol) and mixed with a small amount of N,N-dimethylformamide. The obtained mixed dark green powder was heated for 12 h at 130 °C, resulting in the formation of black powder. XRD were used to measure the temperature dependence of the lattice constant of the black powder. A cylindrical compact was fabricated by uniaxial pressure formation from the black powder. The κ was measured using the laser flash method at RT and 100.4°C. The ρ(T), was measured by the three-terminal method at RT during the first hour and at approximately 40, 60, 80, 105, 135 and 155 °C on a hot plate. The applied voltage was 10 V.

TABLE I.
THERMAL CONDUCTIVITY AT RT AND 100 °C.

	25 °C	100.4 °C
Thermal conductivity ($Wm^{-1}K^{-1}$)	0.68	0.96
Dencity ($g\ cm^{-3}$)	3.926	

III. RESULTS AND DISCUSSIONS

The XRD results showed that the powder was a tetragonal crystal structure after sintering at 30 °C and 50 °C and a cubic structure after sintering at 70 °C, 100 °C and 127 °C. These results are suggesting this powder would exhibit a thermoelectric effect over 60 °C. The coefficient of thermal expansion was calculated to be 44 ppm/K, almost consistent with the reported value of 47.7 ppm/K [3]. The compacts were successfully fabricated by uniaxial pressure formation from the powders (Fig. 1). The high relative densities of over 90 % indicate that a densely packed fabrication was achieved.

The tendency of the ρ(T) decrease with increasing temperature suggests that our fabricated $CH_3NH_3PbI_3$ compact had semiconductor characteristics. Although the ρ(T) at 150 °C decreased one-tenth of that of at RT, the value was still high as a thermoelectric material and needs improvement in the future. On the other hand, the κ of the $CH_3NH_3PbI_3$ compact was measured 0.68 $Wm^{-1}K^{-1}$ at 25 °C and 0.96 $Wm^{-1}K^{-1}$ at 100.4 °C. These values are sufficiently low compared to those of other thermoelectric oxide materials even at 100 °C.

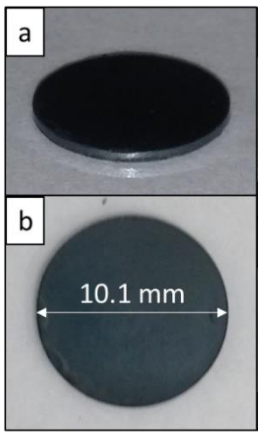

Figue 1. Image of CH_3NH_3I compact, a: side view, b: top view.

REFERENCES

[1] Zeier WG, et al., *Angew. Chem. Int. Ed. Engl.*, 55, 6826-41, 2016.
[2] He Y, Galli G. *Chem. Mater.*, 26, 5394-400, 2014.
[3] Jacobsson, T.J. et al., *Inorg. Chem.*, 54(22), 10678–85, 2015.

Microstructure and Brazing Characteristics of Clad Sheets Fabricated by Vertical-type Tandem Twin-roll Casting

Yusuke Takayama*, Yohei Harada*, Shinji Muraishi* and Shinji Kumai*
*Department of Materials Science and Engineering, Tokyo Institute of Technology, Japan
e-mail: takayama.y.ac@m.titech.ac.jp

Keywords: Twin-roll casting, aluminium clad sheet, brazing sheet, hot roll-bonding

I. INTRODUCTION

Clad strips being laminated several different materials are used in the wide range of industrial fields. However, the fabrication process of the clad strips, such as hot-roll bonding, requires a large amount of time and energy. In order to solve this problem, a vertical-type tandem twin-roll casting (Figure 1) has been developed[1]. The present system is equipped with several twin-roll casters arranged vertically and it can produce the thin clad strips from molten metal directly. This provides great time- and energy saving effects. It was reported that A4045/A3003/A4045 clad strips, for heat exchanger brazing sheets were produced by the present method[2]. During heat exchanger fabrication process, brazing sheets are heated up to melt the overlay. So that the base strip and coolant tube are bonded by overlay filler. In this brazing process, the base strip is eroded by the overlay filler, this phenomenon is called erosion. Excess erosion reduces the mechanical properties and causes the shortage of filler. In this research, the clad sheets fabricated by vertical-type tandem twin-roll casting and hot-roll bonding are used for brazing test and their microstructure and brazing characteristics are compared.

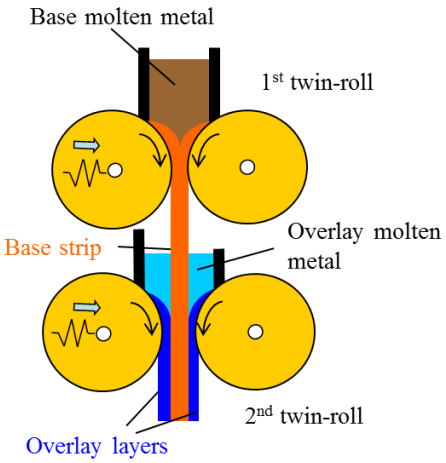

Figure 1 Schematic image of vertical-type tandem twin-roll caster

II. EXPERIMENTAL PROCEDURE

Clad strips with 6 mm thickness consisting of A3003 (Al-1.1 %Mn) for base strip and A4045 (Al-10 %Si) for overlay strip were fabricated by both hot-roll bonding (HRB) and vertical-type tandem twin-roll casting (TRC). The clad strips were provided for the following brazing sheet fabrication process. The clad strips were cold-rolled to 0.17 mm in thickness, subjected to intermediate annealing at 250, 400, 500 °C for 2 h. Annealed sheets were cold-rolled to 0.10 mm in thickness, and without annealing were also prepared. Finally, heat treatment at 600 °C for 3 min which imitated the brazing, was conducted. OM observation and EBSD analysis were made for brazed samples.

III. RESULT AND DISCUSSION

Figure 2 shows the microstructure after brazing for HRB and TRC sheet without intermediate annealing. Remaining base thickness of TRC sheet was larger than HRB. Brazing characteristics of TRC sheets is better than HRB sheets.

Generally, erosion resistance of base strip is improved by grain coarsening after brazing due to the reduction of penetration route of molten overlay[3]. EBSD analysis revealed that grain size was almost the same for HRB and TRC. However, the grains of TRC elongated along the rolling direction reduced the penetration route of molten overlay across the clad interface. This is considered to result in improved erosion resistance.

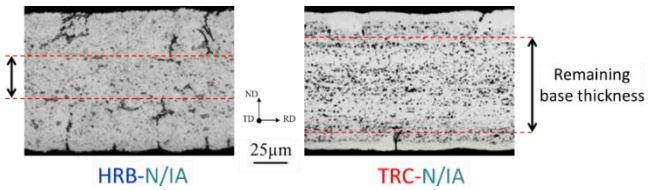

Figure 2 Microstructure after brazing

REFERENCES

[1] T. Haga, et.al., Clad strip casting by a twin roll caster, Proc. 33rd Int. MATADOR Conf. 37, 117, 2009.

[2] Y. Takayama, Y. Harada, S. Kumai, Solidification Manner of Overlay Alloy in Al-Mn/Al-Si Alloy Clad Strips Produced by Vertical-Type Tandem Twin-Roll Casting, in: Proc. 72nd World Foundry Congr., 50, 2016.

[3] J. Qin, S.-B. Kang, J.-H. Cho, Sagging mechanisms in the brazing of aluminum heat exchangers, Scr. Mater., 941 2013.

Grain boundary serration in a Ni-superalloy: on the enhancement of jet engine thermal efficiency

Y. Tang*, A. Wilkinson* and R. Reed**
*Department of Materials, University of Oxford, UK
**Department of Engineering, University of Oxford, UK
e-mail: yuanbo.tang@materials.ox.ac.uk

Keywords: thermal efficiency, creep, grain boundary, superalloy, cavitation

I. INTRODUCTION

Nickel based superalloys are used in extreme conditions, such as aerospace, power generation and nuclear reactors. Their development has significant importance in both economics and environmental aspects for cleaner energy and thermal efficiency. Thermodynamics has proven that thermal efficiency of converting heat into power is proportional to the engine in let temperature. [1] Hence, raising operation temperature of nickel alloys improves engine efficiency in a linear manner.

The properties of a material is hugely dependent on its microstructure, which can be altered correspondingly with different processing routes. By introducing serration in grain boundaries via heat treatment, it has shown promising enhancement in creep life and ductility. [2] However, the strengthening mechanism of the phenomeon is still an open discussion. In this study, we investigate creep properties of Inconel 600, a solid solution alloy, at 3 conditions, to understand solely the effect of grain boundary serration with other variables controlled or eliminated, such as grain size, gamma prime size and distribution, TCP phases, etc. Effect of serration is studied for those conditions where deformation mechanisms changed accordingly. EBSD and X-Ray Tomography were adopted for post mortem quantitative damage analysis. This study shows better understanding of the impact of grain boundary serration in various temperatures and stress levels and it sheds light on a new method of upgrading jet engine efficiency via heat treatment.

II. METHODOLOGY

For generation of serrated and straight grain boundary materials with comparable grain size, 2 heat treatments with slow and rapid cooling rates from above carbide dissolution temperature were employed for each microstructures. 18 standard creep tests were carried out in total where each microstructure were performed with 3 repeat tests at 3 conditions. X-ray tomography was used for visualization and quantification of creep cavitation. EBSD and FEG-SEM were used for further characterisation and strain analysis.

III. RESULTS AND DISCUSSION

Full solution treatment followed by water quenching and controlled furnace cooling have successfully generated two types of different grain boundary morphologies, i.e. straight and serrated. EBSD scanning have shown that both microstructures have comparable grain size and twin fractions. Creep test results in Figure 1 illustrates that with increasing temperature from 700 to 900° C, a huge drop in ductility has been observed, which suggested a change in deformation mechanism. In all conditions observed, serrated grain boundary has proven enhancement of creep life and ductility in all cases, particularly in condition of 815° C/70MPa and 900° C/40MPa. X-Ray Tomography results highlighted that cavitation behaviour become pronounced with increasing temperature and decreasing stress, as shown by total cavitation volume and largest cavity size before failure. This is due to serration impedes effectively on cavity growth and crack propagation.

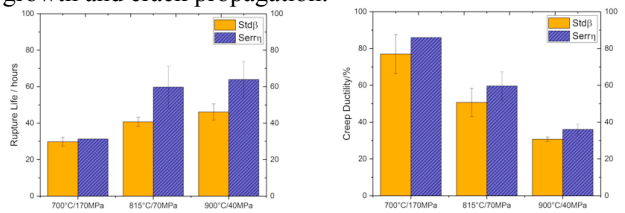

Figure 1. (a) creep rupture life, and (b) ductility of straight and serrated grain boundary at 3 conditions, where Stdβ and Serrη represents straight and serrated grain boundary samples repectivley.

IV. SUMMARY

Heat treatment has shown the possibility of changing grain boundary morphologies in a nickel alloy and creep properties can be improved correspondingly. Creep rupture life and ductility are enhanced particularly in higher temperature and lower stress regime due to stronger cavitation resistance by serrated grain boundaries. The results can be further applied to other superalloys for particular applications with improvement of operation temperature and jet engine thermal efficiency as ultimate goals.

V. REFERENCES

[1] M. Moran, H. Shapiro, D. Boettner, M, Bailey, *Fundamentals of Engineering Thermodynamics, 1987.*

[2] P. Kontis, H. Yusof, S. Pedrazzini, M. Danaie, K. Moore, P. Bagot, M. Moddy, C. Grovenor, R. Reed, *Acta Meterialia, 103, 2016.*

Development of a Throated Downdraft Gasifier Test-Bed for Evaluating Gasifier Control Systems

Zakir Khan* and Ian Watson
*System, Power and Energy, School of Engineering, University of Glasgow, UK
zakir.kahn@glasgow.ac.uk
Keywords: throated, downdraft, fixed bed, control, design

I. INTRODUCTION

The primary objective of this study is to develop a downdraft gasifier test-bed to evaluate gasification of various biomass feedstocks, tar detection systems and gasifier control strategies. The development process consisted of optimising the gasifier dimensions through empirical relationships, the physical properties of the biomass and experimental data in the literature. The two most important dimensions to evaluate were the throat diameter, the smallest dimension in the gasifier, and the diameter of the gasifier. Other important design parameters were the hearth load and gasification rate used for eventuating the gasifer throat and overall diameter. An optimum Equivalence Ratio (ER) of 0.3 was considered to evaluate the total air required for the gasification process, considering the physical properties of local *Miscanthus* pellets and gasification reactions. Once the throat diameter and gasifer diameter were evaluated, the reactor height was evaluated based on the total volume occupied by the *Miscanthus* with the mass flow rates used for initial gasifier dimensions. Furthermore, the nozzle size and number of nozzles was evaluated with respect to the throat size. A 3-D design model was carried out in SolidWorks 2014. The design and fabrication strategy of the gasifer was to enable a flexible system to allow rapid changes of the design elements, allowing gasifier optimisation for different feedstocks. The upper part comprised a straight cylinder and the throat geometry. The lower part, connected via a flange assembly, contained the char grate. Different mesh sizes for the grate can be used to investigate its effect on gas quality.

A. Design Strategy

The aim of the design process is to evaluate different dimensions through empirical relationships with the help of experimental data. The two important dimensions to evaluate are throat diameter, the smallest dimensions in the gasifier, and the diameter of a gasifier. The throat diameter design strategy is shown in the Figure 1. The important design parameters are the hearth load and gasification rate. The hearth load defines the throat diameter along with total gas produced through oxidation and gasification reaction based on the biomass properties (proximate and ultimate properties). Similarly, the gasification rate defines the diameter of the gasifier. Initially, the downdraft air gasification system considers

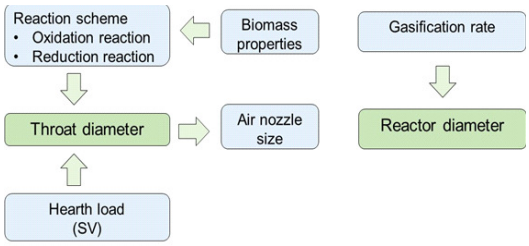

Figure 1. Design strategy for throated downdraft gasifier [1]

equivalence ratio (ER) as the main variable whereas the temperature variation in the system depends on the equivalence ratio (ER). ER can be defined as the ratio of $(A/F)_{actual}$ to $(A/F)_{stoich}$ where A and F represents air and fuel. With the reference to optimum value of 0.3 (nearby) in the literature [2, 3], the present design study considers ER of 0.30 for the design evaluation of throat.

II. RESULTS AND DISCUSSIONS

The design rating, operating conditions, and basic design specifications are presented in Table 1. The design rating of 3-4 kW is considered due to the lab scale size of the gasifier. Stainless steel (SS) 310 was used as the material of construction which is preferred over SS 316 (pipe) due to better resistant capabilities to oxidation at high temperature (T >1000 °C). In addition, air nozzle, flanges and the grate are fabricated from SS 310 bar.

TABLE I.
DESIGN SPECIFICATION OF DOWNDRAFT GASIFIER

Parameter	Value
Design rating	3.4 kW
Biomass feed (continuous)	0.7 kg/h
Air flow rate (0.20-0.40 ER)	0.87-1.3 kg/h
Gasifier diameter (ID)	70 mm
Gasifier height (with flanges)	720 mm
Throat diameter	31 mm
Throat height (with annulus height)	60 mm
Throat angle	60°
Ash grate diameter (ID)	70 mm
Orifice size (ash grate)	2 mm

References

[1] T. Reed, S. Ellis, A. Das, S. Deutch, "Superficial velocity - the key to downdraft gasification," in *4th Biomass Conference of the Americas*, Oakland, CA, USA, 1999.

[2] P. Lv, Z. Yuan, L. Ma, C. Wu, Y. Chen, and J. Zhu, "Hydrogen-rich gas production from biomass air and oxygen/steam gasification in a downdraft gasifier," *Renewable Energy,* vol. 32, pp. 2173-2185, 10// 2007.

[3] F. M. Guangul, S. A. Sulaiman, and A. Ramli, "Gasifier selection, design and gasification of oil palm fronds with preheated and unheated gasifying air," *Bioresource Technology,* vol. 126, pp. 224-232, 12// 2012.

5. Campus Map

James Watt South Building marked A1 on the campus map, available from the link below:

http://www.gla.ac.uk/media/media_335384_en.pdf

Campus map

Accommodation Services	E2	James Watt South Building	A1
Adam Smith Building	D8	Joseph Black Building	B4
Archive Services	C7	Kelvin Building	B8
BHF Glasgow Cardiovascular Research Centre	C12	Kelvin Gallery	A7
(Glasgow) Biomedical Research Centre – Sir Graeme Davies Building	C13	Library	D11
		Lilybank House	D9
		McGregor Building	C11
		McIntyre Building	A22
Bower Building	B7	McMillan Reading Room	E1
Boyd Orr Building	D1	Main Building	A10
Bute Hall	A13	Main Gatehouse	A21
Careers Service	E2	Mathematics & Statistics Building	C3
Catholic Chaplaincy	E11	Pearce Lodge	A4
Chapel	A8	Principal's Lodging	A18
Chaplaincy	A24	Queen Margaret Union	D3
Communications & Public Affairs Office	A20	Randolph Hall	A10
		Rankine Building	E7
Concert Hall	A12	Registry	E2
Conferences & Events	B6	Research, Strategy & Innovation Office	A19
Davidson Building	B1	Robertson Building	C2
Development & Alumni Office	A20	Sir Alexander Stone Building	D5
Disability Service	E12	Sir Alwyn Williams Building	D20
East Quadrangle	A5	Sir Charles Wilson Building	E15
Florentine House	E4	Southpark House	E5
Fraser Building	E2	St Andrew's Building	E14
Gilchrist Postgraduate Club	A26	Stair Building	A19
Gilmorehill Halls	E9	Stevenson Building	E6
Glasgow International College	C1	Student Services Enquiries Desk	E2
Glasgow University Union	E8	West Medical Building	B2
Graham Kerr Building	B3	West Quadrangle	A6
Gregory Building	D2	Western Infirmary Lecture Theatre	B9
Hetherington Building	D10	Wolfson Building	B10
Hunter Halls	A14	Wolfson Medical School Building	C8
Isabella Elder Building	B6		
IT Services	A2		
James Watt North Building	A2		

James Watt South Building Entrance

6. Restaurants

Please be prompt for restaurant bookings

Thursday 7th September

18:00-19:30 Evening Reception, **Baffo Pizza and Birra**, 1377 Argyle St, Glasgow, G3 8AF
Tel: 0141 583 0000

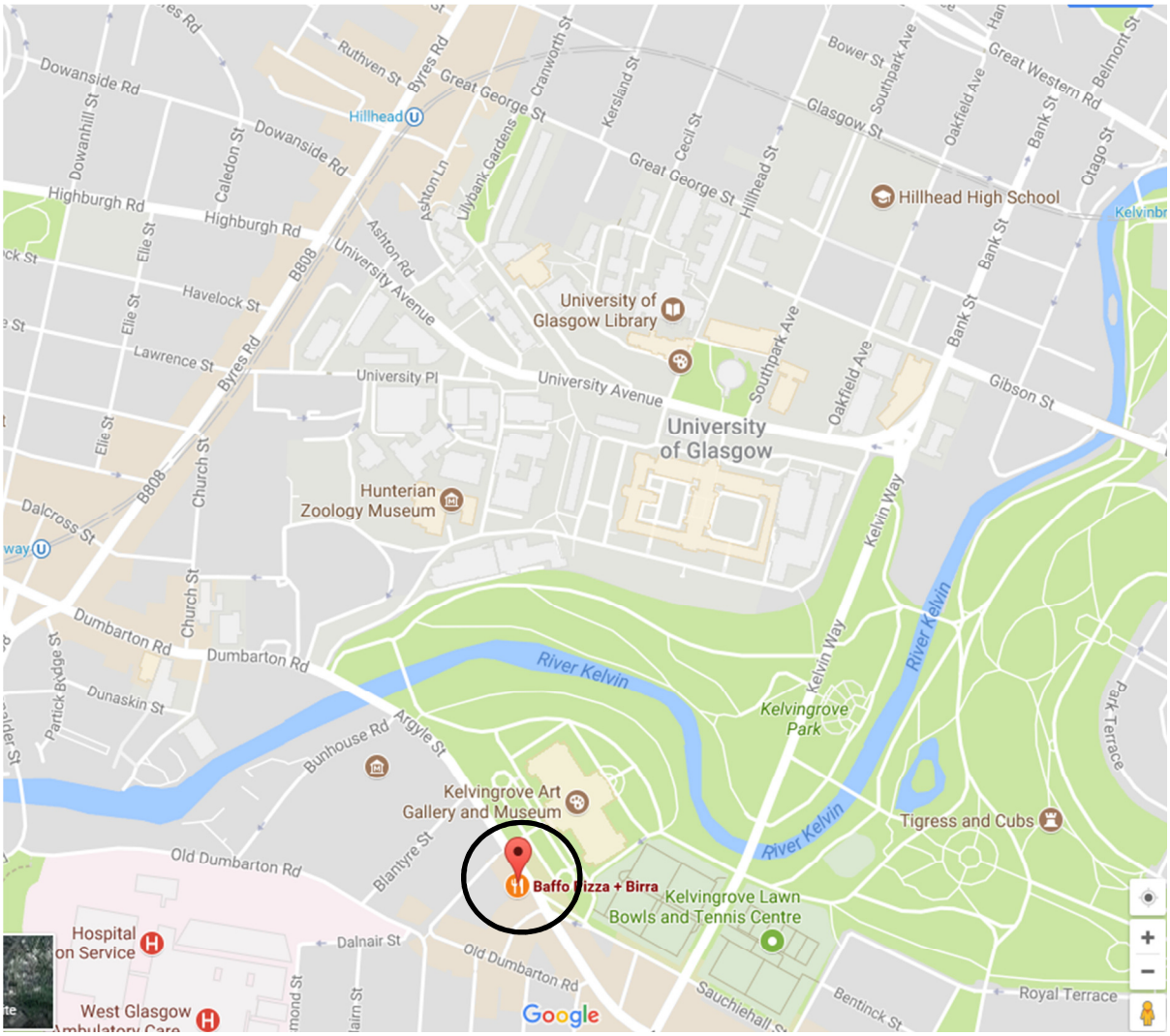

Friday 8th September

17:30-19:30 Reception, **Ubiquitous Chip**, 12 Ashton Lane, Glasgow, G12 8SJ
Tel: 0141 334 5007.

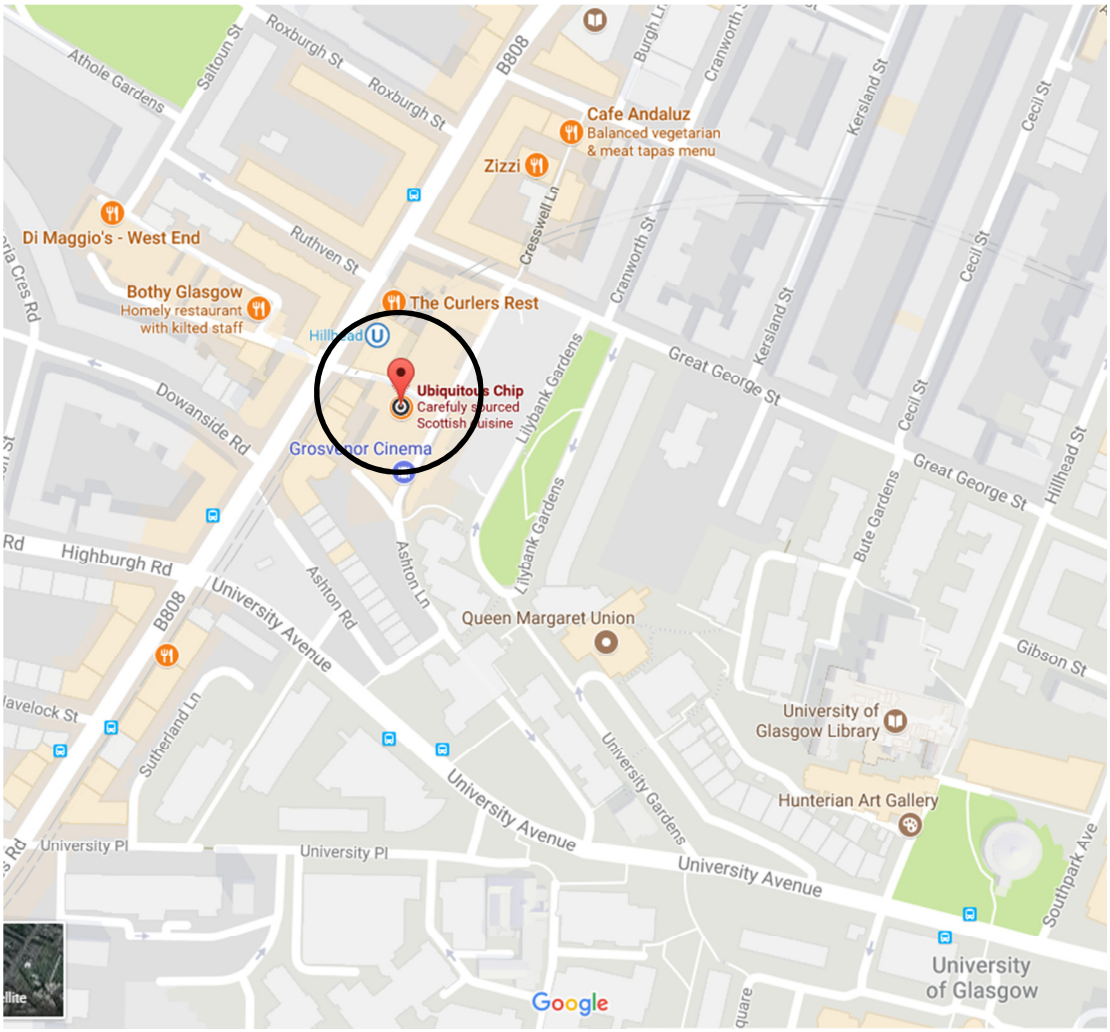

Saturday 9th September

17:45 19:15 Mini Grill, 244 Bath Street, Glasgow, G2 4JW

Tel: 0141 332 2732